Polar Geosci., **19**, 62–88, 2006

Geochemistry of mafic metamorphic rocks in the Lützow-Holm Complex, East Antarctica: Implications for tectonic evolution

Yoshimitsu Suda[1]*, Shin-ichi Kagashima[2], M. Satish-Kumar[3], Yoichi Motoyoshi[1] and Yoshikuni Hiroi[4]

[1]*National Institute of Polar Research, Kaga 1-chome, Itabashi-ku, Tokyo 173-8515*
[2]*Department of Earth and Environmental Sciences, Faculty of Science, Yamagata University, Kojirakawa-machi 1–4–12, Yamagata 990-8560*
[3]*Institute of Geosciences, Shizuoka University, Oya 836, Suruga-ku, Shizuoka 422-8529*
[4]*Department of Earth Sciences, Faculty of Science, Chiba University, Yayoi-cho 1–33, Inage-ku, Chiba 263-8522*
**Corresponding author. E-mail: suda@nipr.ac.jp*

(Received March 27, 2006; Accepted June 19, 2006)

Abstract: Mafic metamorphic rocks are widely distributed through the Lützow-Holm Complex (LHC) of East Antarctica, as layers between or enclaves within metasedimentary and metaigneous lithologies. It has been inferred that the peak metamorphic grade of the LHC progressively increases in a southwestern direction from amphibolite-facies to granulite-facies conditions, with mineral assemblages in the mafic metamorphic rocks changing from hornblende (magnesiohornblende)±biotite+plagioclase to orthopyroxene+clinopyroxene±hornblende (pargasite, magnesiohastingsite and tschermakite)±biotite±garnet+plagioclase. Field relationships suggest that amphibolite-grade mafic metamorphic rocks derive from mafic magma intruded into metasedimentary units, whereas granulite-facies mafic metamorphic rocks are a mixture of detrital blocks and mafic sill or intrusions.

Major and trace element compositions of mafic metamorphic rocks are similar to those of igneous rocks of tholeiite affinity, and can be divided into volcanic-arc basalt (VAB)-type or mid-ocean ridge basalt (MORB)-type compositions. On a regional scale, VAB-type lithologies are predominant in amphibolite-facies areas, and MORB-type lithologies predominate in granulite-facies areas. On the basis of HFSE concentrations and Nb/Y ratios, MORB-type lithologies have T-type and E-type MORB compositions with oceanic plateau basalt and back-arc basin basalt affinities, and are occasionally found in the field intercalated with metasedimentary layers, characteristic of magmatism and sedimentation cycles in a marginal sea basin setting. Such field relationships provide information on the tectonic environment of protolith formation in the LHC. Various crustal components have been amalgamated into a relatively narrow mobile belt, which was subjected to high-grade metamorphism during the final closure of oceanic basins as a result of continent–continent collision.

key words: mafic metamorphic rocks, geochemistry, Lützow-Holm Complex, East Antarctica

1. Introduction

The Lützow-Holm Complex (LHC) is a high-grade mobile belt extending along the coastline in Lützow-Holm Bay and the Prince Olav Coast between longitudes 37° and 45°E (Fig. 1a, b). The complex is composed of high-grade metamorphic rocks and mafic to felsic dykes. Metamorphic lithologies include pelitic and psammitic felsic gneiss, quartzo-feldspathic gneiss, mafic to intermediate metamorphic rocks with subordinate ultramafic rock, marble, calc-silicate rock and granitic gneiss. Hiroi *et al.* (1983a, 1991) suggest that the LHC experienced medium-pressure metamorphism through a clockwise *P-T-t* path, where early-formed kyanite in metapelite was replaced by sillimanite at peak temperatures and by rare andalusite during cooling. Peak metamorphic mineral assemblages increase along the LHC from amphibolite-facies in the NE part through transitional granulite in the central part to granulite-facies in the SW part (Fig. 1b). Peak pressure and temperature conditions have been estimated to be 6.0–8.7 kbar and 700–850°C across the LHC (Hiroi *et al*., 1983a, 1987, 1991; Shiraishi *et al*., 1984). Recent studies indicate higher *P-T* conditions in the SW part of the complex, of 7–11 kbar and 810–960°C at Skallevikhalsen (Yoshimura *et al*., 2004), and 9–11 kbar and 950–1040°C at Rundvågshetta (Motoyoshi and Ishikawa, 1997).

Numerous geochronological studies have concluded that peak metamorphism in the LHC occurred between 560 Ma and 520 Ma (U-Pb zircon SHRIMP ages by Shira-

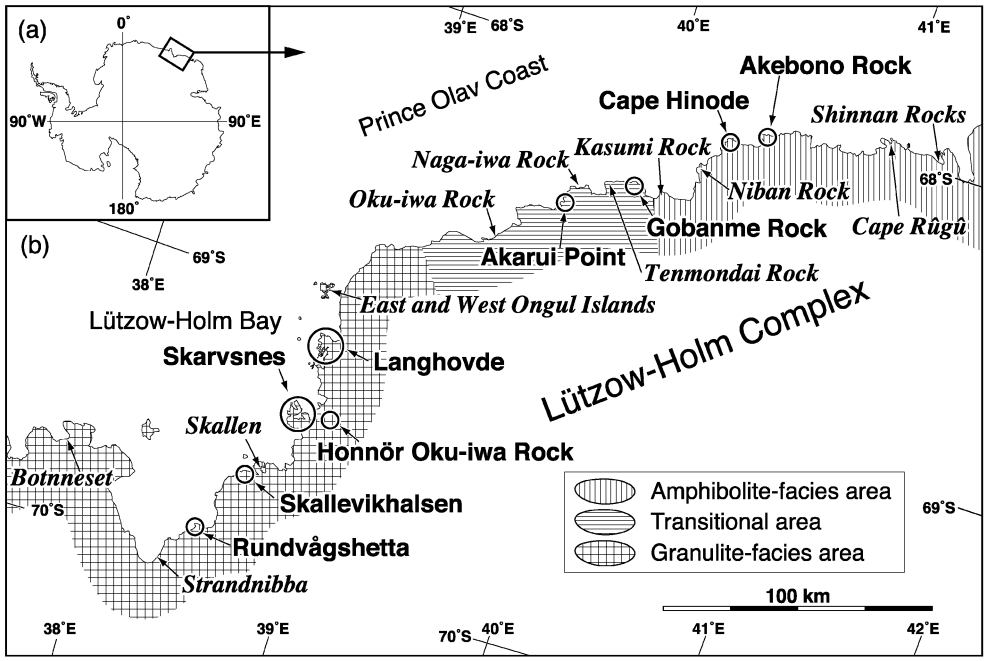

Fig. 1. (a) Map of Antarctica. (b) Map of Lützow-Holm Complex showing the localities of samples analyzed in this study (in bold letters) and previous studies (in italic letters). Metamorphic areas: amphibolite-facies area, transitional area and granulite-facies area, are after Hiroi et al. (1983a).

ishi *et al*., 1994, 2003; Fraser, 1997). Metamorphic protolith ages or sources of detrital zircon ages are ~1000 Ma (U-Pb ages of inherited core of zircons by Shiraishi *et al*., 1994, 2003; Fraser, 1997 and Rb-Sr whole rock isochron ages by Nakajima *et al*., 1987). Granitic magmatism is also indicated at *ca.* 670 Ma from Rb-Sr and Sm-Nd whole-rock isochron ages (Nishi *et al*., 2002).

Kanisawa *et al.* (1987) reported that mafic metamorphic rocks in the LHC have MORB affinities. Hiroi *et al.* (1986) suggested that metamorphosed ultramafic rocks originated as cumulate fractionated from tholeiitic magma. These studies suggest that the mafic and ultramafic rocks represent remnants of oceanic floor lithologies.

During the summer season of the 46th Japanese Antarctic Research Expedition (JARE-46; 2004–2006), we carried out geological field surveys in the LHC. This study will focus on mafic metamorphic rocks from Akebono Rock, Cape Hinode, Gobanme Rock, Akarui Point, Langhovde, Skarvsnes, Honnör Oku-iwa Rock, Skallevikhalsen and Rundvågshetta. We describe field occurrences, petrography and geochemistry, in order to derive tectonic scenarios from protolith compositions.

2. Field occurrences

Mafic metamorphic rocks throughout the LHC occur as dark layers, lens and blocks, which are concordant with the gneissosity of the host rocks. In contrast, low-grade or unmetamorphosed mafic rocks occur as dykes that intrude across gneissosity in the host rocks. In this study, we concentrate on pre- to syn-metamorphic units. On the basis of field relationships, mafic metamorphic rocks are regionally divided into three groups as described below.

2.1. Amphibolite-facies area (NE part of the LHC): Akebono Rock and Cape Hinode

The mafic metamorphic rocks at Akebono Rock occur as layers alternating with biotite gneiss, hornblende biotite gneiss and granitic gneiss (Fig. 2a–c). These layers have thicknesses that vary from a few centimeters to several meters. The boundary between the mafic metamorphic rocks and the surrounding gneisses are blurred and irregular (Fig. 2b). Figure 2c shows an outcrop where a mafic protolith has been intruded into biotite gneiss, and in turn is intruded by a granitic protolith prior to further metamorphism and deformation.

Mafic metamorphic rocks at Cape Hinode have three modes of occurrence. The first type occurs in the eastern part of Cape Hinode, as folded decimeter-long layers

Fig. 2 (opposite). Modes of occurrence of mafic metamorphic rocks (amphibolite and mafic granulite). (a) Amphibolite and biotite-hornblende gneiss in Akebono Rock. (b) Close-up view of boundary between amphibolite and biotite-hornblende (bt-hbl) gneiss in Akebono Rock. (c) Field relation between biotite (bt) gneiss, granitic (Gr) gneiss and amphibolite (amph) in Akebono Rock. (d) Alternation of amphibolite and biotite gneiss in Gobanme Rock. (e) Alternation of amphibolite and biotite gneiss in Akarui Point. (f) Alternation of quartzo-feldspathic, pelitic and mafic granulite, and quartzo-feldspathic garnet biotite (grt-bt) gneiss in Skallevikhalsen. (g) Block of mafic metamorphic rocks in charnockitic pyroxene gneiss in Rundvågshetta. (h) Schlieren of mafic granulite in charnockitic pyroxene gneiss in Rundvågshetta.

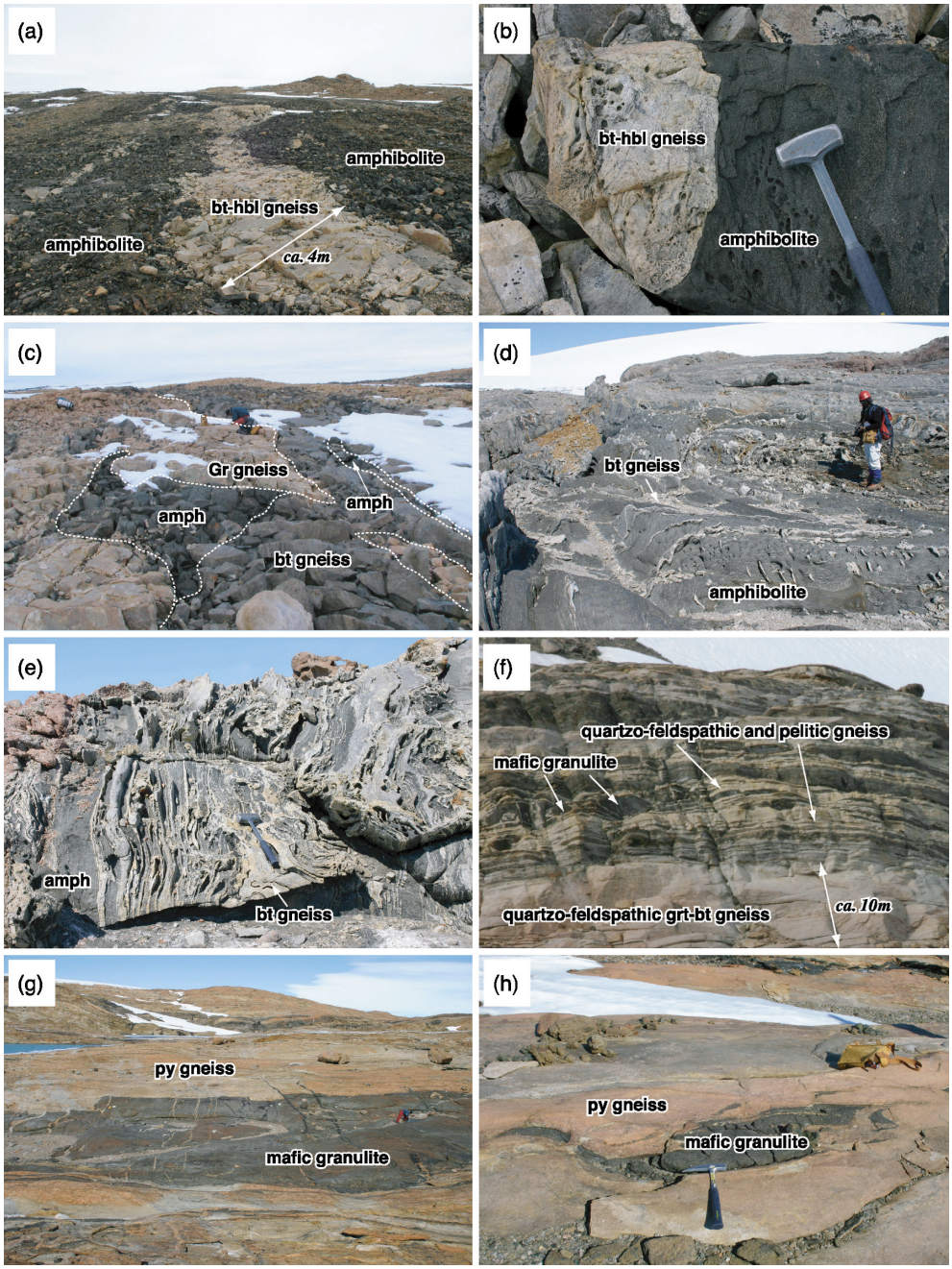
(a)
amphibolite
bt-hbl gneiss
amphibolite
ca. 4m
(b)
bt-hbl gneiss
amphibolite
(c)
Gr gneiss
amph
amph
bt gneiss
(d)
bt gneiss
amphibolite
(e)
amph
bt gneiss
(f)
quartzo-feldspathic and pelitic gneiss
mafic granulite
quartzo-feldspathic grt-bt gneiss
ca. 10m
(g)
py gneiss
mafic granulite
(h)
py gneiss
mafic granulite

Fig. 2.

within hornblende gneiss. The second type occurs as decimeter-long lenses and enclaves in anorthositic gneiss. The third type occurs as tens of meters-scale amphibolite bodies in southwestern Cape Hinode. Amphibolite contains a foliation defined by aligned mafic mineral grains, along with quartzo-feldspathic and pyroxenes-rich patches. Numerous felsic pegmatite dykes intrude into amphibolite bodies.

2.2. Transitional area (central part of the LHC): Gobanme Rock and Akarui Point

The mafic metamorphic rocks at Gobanme Rock occur as decimeter- to several meter-scale layers alternating with hornblende gneiss, biotite gneiss, garnet-biotite gneiss, in which many open and tight folding structures are characteristically observed. Centimeter-scale quartzo-feldspathic pods occur along the fold hinges indicating foliation-boudinage type of earlier granitic melt segregation (Fig. 2d).

The mafic metamorphic rocks at Akarui Point occur either as centimeter to decimeter-scale thin layers alternating with biotite-hornblende gneiss or as decimeter- to meter-scale blocks and lenses in biotite-hornblende gneiss. Thin layers are deformed into open to tight folds (Fig. 2e). Decimeter- to meter-scale lenses and blocks of ultramafic and calc-silicate gneiss are also observed in the biotite-hornblende gneiss.

2.3. Granulite-facies area (SW part of the LHC): Langhovde, Skarvsnes, Honnör Oku-iwa Rock, Skallevikhalsen and Rundvågshetta

Pyroxene gneiss (charnockite) is abundant in this region, along with decimeter- to meter-scale blocks of calc-silicate and ultramafic gneiss. The field relationships of mafic metamorphic rocks from Langhovde, Skarvsnes and Honnör Oku-iwa Rock are almost identical, occurring as layers, schlieren, lenses and blocks in hornblende gneiss, garnet gneiss, garnet-biotite gneiss and pyroxene gneiss. Most mafic metamorphic bodies are hosted by pyroxene gneiss. Mafic layers are often boudinaged forming schlieric patches and flattened lenses. Schlieren are centimeters to decimeters long; blocks and lenses are centimeters to meters in length.

The mafic metamorphic rocks at Skallevikhalsen occur as decimeter-scale thin layers alternating with garnet-biotite gneiss and quartzo-feldspathic gneiss, or as meter-scale thick layers alternating with layers of marble and pelitic gneiss. Continuous layers of mafic gneiss are typically boudinaged into blocks and lenses (Fig. 2f).

The mafic metamorphic rocks at Rundvågshetta occur as several meter-scale thick layers and blocks (Fig. 2g), or as decimeter-scale thin layers, schlieren and lenses (Fig. 2h), which occur predominantly in pyroxene gneiss. Layers within the mafic gneisses characterized by the size and abundance of garnet porphyroblasts are abundant in this region, along with decimeter- to meter-scale blocks of calc-silicate and ultramafic gneiss. The field relationships of mafic metamorphic rocks from Langhovde, Skarvsnes and Honnör Oku-iwa Rock are almost identical, occurring as layers, schlieren, lenses and blocks in hornblende gneiss, garnet gneiss, garnet-biotite gneiss and pyroxene gneiss. Most mafic metamorphic bodies are hosted by pyroxene gneiss. Mafic layers are often boudinaged forming schlieric patches and flattened lenses. Schlieren are centimeters to decimeters long; blocks and lenses are centimeters to meters in length.

The mafic metamorphic rocks at Skallevikhalsen occur as decimeter-scale thin layers alternating with garnet-biotite gneiss and quartzo-feldspathic gneiss, or as meter-

scale thick layers alternating with layers of marble and pelitic gneiss. Continuous layers of mafic gneiss are typically boudinaged into blocks and lenses (Fig. 2f).

The mafic metamorphic rocks at Rundvågshetta occur as several meter-scale thick layers and blocks (Fig. 2g), or as decimeter-scale thin layers, schlieren and lenses (Fig. 2h), which occur predominantly in pyroxene gneiss. Layers within the mafic gneisses are characterized by the size and abundance of garnet porphyroblasts.

2.4. Possible precursors for the mafic metamorphic rocks

Due to high-grade metamorphism and intense polyphase deformation we can only speculate about possible precursors for the mafic metamorphic rocks. Only a few relics inferring metamorphosed equivalents of intrusive dykes or sills are found in Akebono Rock. The meter-size layers and lens of mafic metamorphic rocks in other occurrences are associated with supracrustal rocks such as calc-silicates and quartzite, which may represent tectonic relics of high-grade metamorphic rocks and are grouped into volcano-sedimentary lithological units.

3. Petrography

3.1. Mineral assemblages

Mineral assemblages observed in mafic metamorphic rocks of the LHC are listed in Table 1. Main constituent minerals are hornblende, clinopyroxene, orthopyroxene, biotite, garnet, plagioclase and quartz. Accessory minerals are apatite, epidote, titanite, chlorite and Fe-Ti oxides and sulfides. Titanite and apatite are found in all mafic lithologies. Fine needles of epidote (*ca.* 0.2 mm in length) occur in mafic rocks from Akebono Rock, as inclusions in plagioclase or hornblende (Fig. 3a). K-feldspar is found as fine-grained (*ca.* 0.1 mm) inclusions in plagioclase (Fig. 3a). Quartz is more abundant in mafic rocks from the amphibolite-facies area.

The dominant mineral assemblage in the LHC varies from plagioclase–hornblende assemblage (*i.e.*, amphibolite) to clinopyroxene–orthopyroxene–plagioclase (*i.e.*, mafic granulite), consistent with the three metamorphic domains defined by Hiroi *et al.* (1983a) (Fig. 1b). Exceptionally, mafic granulite is found at Cape Hinode (Fig. 3d), which occurs in the amphibolite-facies area as defined by Hiroi *et al.* (1983a) (Fig. 1b). Recent studies suggest that Cape Hinode represents an allochthnous unit in the LHC, on the basis of geochronological data (*i.e.*, yields distinct ages of *ca.* 1000 Ma; Shiraishi *et al.*, 1995) and granulite-grade mineral assemblages (Hiroi *et al.*, 2006).

3.2. Mineral reaction textures

Constituent minerals in the mafic metamorphic rocks form foliated or granoblastic fabrics that indicate complete metamorphic recrystallization. Aligned, millimeter-long grains of hornblende, biotite and pyroxene define foliation (Fig. 3b, e, h). Elsewhere hornblende and pyroxene grains 0.5–1 mm across occur in a granoblastic fabric (Fig. 3g). The rims of clinopyroxene grains in rocks from Akebono Rock are often altered to hornblende, due to hydrating retrograde reactions during cooling (Fig. 3c). Garnet porphyroblasts 2–5 mm across in rocks from Skallevikhalsen and Rundvågshetta are commonly surrounded by symplectites of plagioclase, orthopyroxene and magnetite

Table 1. Mineral assemblages of mafic metamorphic rocks from the LHC.

Sample No.	Analysis No.	Locality	Area	Rock type	cpx	opx	hbl	grt	bt	pl	qtz	Accessary minerals
SU04122504A, B	3, 33	AR	AF	amph			++		tr	+	+	ep, ap, tit, om
SU04122503B, C	7, 32	AR	AF	amph			++			++	+	om
SU04122601A, B	35, 36	AR	AF	bt amph			++		+	+	tr	ap
SU04122601D	38	AR	AF	cpx amph	+		++			++	tr	ep, tit
SU04121905	40	CH	AF	cpx amph	+		++		tr	++		ap
SU04122004-1	44	CH	AF	hbl granul	+	+	++			++		
SU05010302	10	AP	T	amph			++		tr	++	+	ap
SU05010307	11	AP	T	bt amph			++		+	+	+	ap, om
SU05010301E	76	AP	T	cpx amph	+		++		tr	++	+	om
SU05010309B	78	AP	T	cpx amph	+		++		tr	+	+	ap, tit, om
SU05010422	79	AP	T	bt amph			++		+	+	+	om
SU05020702	82	LA	GF	bt granul	+	+			+	++		ap, om
SU05012806	86	HO	GF	bt granul	+	+			+	++		om
SU05012501A, B	87, 88	SVN	GF	hbl granul	+	+	++		tr	+		
SU05013009	89	SVN	GF	bt-hbl granul	+	+	+		+	++		ap, om
SU05011807A, B	14, 94	SVH	GF	grt-hbl granul	+	+	+	+		+	tr	om
SU05011805	92	SVH	GF	hbl granul	+	+	++			+		om
SU05011806	93	SVH	GF	bt-hbl granul	+	+	+		+	+		om
SU05011809	95	SVH	GF	hbl granul	+	+	+			++		om
SU05011901	96	SVH	GF	bt-hbl granul	+	+	+		+	++		ap, om
SU05012003B	100	SVH	GF	hbl granul	+	+	++		tr	+		ap, om
SU05012004, 06	101, 102	SVH	GF	bt amph			++		+	++	tr	ap, om
SU05012007	103	SVH	GF	hbl granul	+	+	+		+	+	tr	om
SU05012013	105	SVH	GF	cpx amph	+		++			+		om
SU05012105	108	SVH	GF	bt amph			++		+	+		ap, om
SU05011001, 02	16, 109	RVH	GF	bt-hbl granul	+	+	tr		+	+		ap
SU05011003B	17	RVH	GF	bt granul	++	+			+	+		ap, om
SU05011004	110	RVH	GF	bt-hbl granul	+	+	++		+	+		
SU05011005B	111	RVH	GF	bt-hbl granul	+	+	+		tr	++		om

Rock type abbreviations: amph; amphibolite, granul; granulite.

Mineral abbreviations: cpx; clinopyroxene, opx; orthopyroxene, hbl; hornblende, grt; garnet, bt; biotite, pl; plagioclase, qtz; quartz, ap; apatite, om; opaque minerals, ep; epidote, ap; apatite, tit; titanite, om; opaque minerals.

Locality abbreviations: AR; Akebono Rock, CH; Cape Hinode, GR; Gobanme Rock, AP; Akarui Point, LA; Langhovde, HO; Honnör Oku-iwa Rock, SVN; Skarvsnes, SVH; Skallevikhalsen, RVH; Rundvågshetta.

Area abbreviations: AF; amphibolite-facies area, T; transitional area, GF; granulite-facies area.

++; abundant (>30 modal %), +; common (5–30 modal %), tr; minor (< 5 modal %).

Fig. 3 (opposite). Photomicrographs showing mineral textures of mafic metamorphic rocks. (a) Needles of epidote and fine-grained inclusions of K-feldspar in amphibolite (SU04122601D) from Akebono Rock. (b) Elongate shape of hornblende and biotite in amphibolite (SU05010307) from Akarui Point. (c) Clinopyroxene replaced by hornblende in amphibolite (SU04122601D) from Akebono Rock. (d) Orthopyroxene in mafic granulite (SU04122004-1) from Cape Hinode. (e) Elongated shape of biotite in mafic granulite (SU05011003B) from Rundvågshetta. (f) Symplectite of orthopyroxene and plagioclase around garnet in mafic granulite (SU05011807A) from Skallevikhalsen. (g) Granoblastic texture of orthopyroxene and plagioclase from Rundvågshetta (SU05011200B). (h) Elongated shape of biotite overprinted in hornblende in amphibolite (SU05012105) from Skallevikhalsen. (a) crossed polars, (b–h) plane polarized light. Mineral abbreviations are the same as in Table 1.

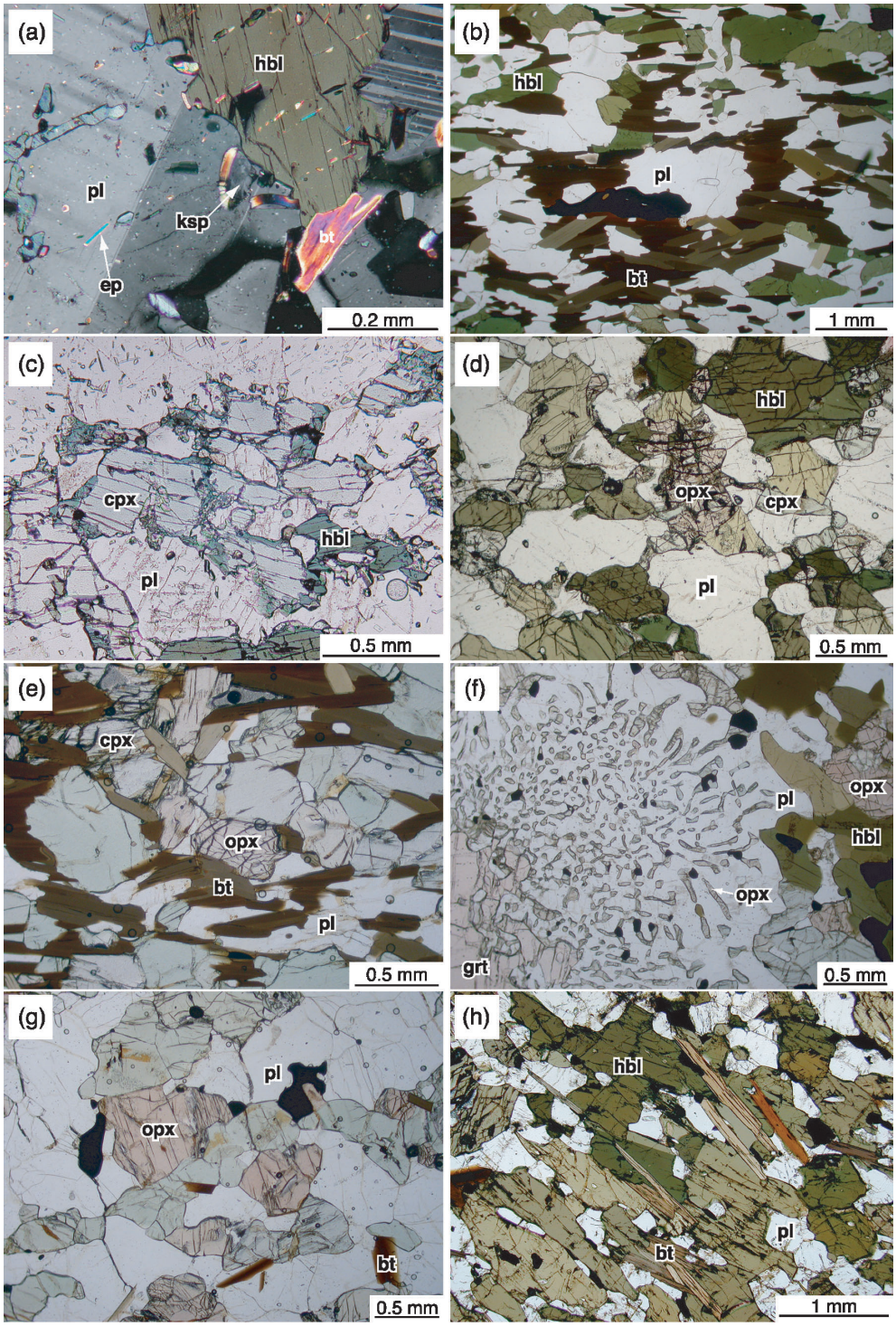
(a)
hbl
pl
ksp
bt
ep
0.2 mm
(b)
hbl
pl
bt
1 mm
(c)
cpx
hbl
pl
0.5 mm
(d)
hbl
opx
cpx
pl
0.5 mm
(e)
cpx
opx
bt
pl
0.5 mm
(f)
pl
opx
hbl
opx
grt
0.5 mm
(g)
pl
opx
bt
0.5 mm
(h)
hbl
pl
bt
1 mm

Fig. 3.

(Fig. 3f), characteristic of decompression reactions (Motoyoshi, 1986; Fraser *et al*., 2000). Elongated shape of coarse-grained biotite appears to overprint the foliation defined by hornblende (Fig. 3h).

3.3. Mineral chemistry

3.3.1. Analytical method

Chemical compositions of orthopyroxene, clinopyroxene, amphibole, plagioclase, biotite, garnet, epidote and opaque minerals in mafic metamorphic rocks from the LHC were analyzed using a wavelength dispersive electron-probe microanalyzer (JEOL JCMA-7800) at the National Institute of Polar Research (NIPR). The operating conditions were a 12 nA beam current, 15 kV accelerating voltage and 5 μm beam diameter. Representative chemical compositions of the minerals are listed in Table 2.

3.3.2. Pyroxenes

Most X_{Mg} values of orthopyroxene range between 0.46 and 0.59, and Al (pfu) contents vary between 0.02 and 0.06. Exceptionally, orthopyroxene of higher X_{Mg} values (0.62–0.64) occurs in a sample from Rundvågshetta. Orthopyroxene of lower X_{Mg} (0.44–0.46) and higher Al (pfu) content (0.05–0.07) occur in samples from Skallevikhalsen. Chemical zoning is found in some orthopyroxene grains, where Al content decreases from core to rim.

The majority of X_{Mg} values of clinopyroxene range between 0.62 and 0.77, and Al (pfu) contents vary between 0.04 and 0.12. Clinopyroxene of higher X_{Mg} values (0.75–0.80) and higher Al (pfu) content (0.09–0.16) occur in a sample from Cape Hinode, whereas clinopyroxene of lower X_{Mg} values (0.57–0.63) occur in the samples from Skallevikhalsen. Chemical zoning is found in some clinopyroxene, where Al decreases from core to rim.

3.3.3. Amphibole

The structural formulae of amphiboles are calculated based on 23 oxygens per unit cell, and the Fe^{2+}/Fe^{3+} ratio was estimated on the basis of total cations excluding Ca, Na and K (Leake *et al*., 1997) (Table 2). Following the nomenclature by Leake *et al.* (1997) (Fig. 4), amphiboles are predominantly magnesiohornblende at Akebono Rock (amphibolite-facies), magnesiohastingsite and pargasite in Skarvsnes and Skallevikhalsen (granulite-facies). At Akarui Point (transitional granulite) and Cape Hinode (amphibolite-facies), amphiboles range from magnesiohornblende–edenite through tschermakite–magnesiohastingsite to pargasite. Amphiboles from amphibolite and transitional granulite host rocks have lower Ti (pfu) contents (0.04–0.25) and higher $Mg/(Mg+Fe^{2+})$ ratios (0.58–0.79) than those from granulite-facies rocks (0.21–0.30 pfu Ti, 0.50–0.68 $Mg/(Mg+Fe^{2+})$). Chemical zoning is found in some grains, where Ti and Al contents decrease from core to rim.

3.3.4. Biotite

Biotite becomes enriched in Ti with increasing grade, from 0.26–0.30 pfu in amphibolite-facies hosts (Akebono Rock), 0.31–0.53 pfu in transitional granulites (Akarui Point), to 0.45–0.75 pfu in granulite-facies hosts (Langhovde; Honnör Oku-iwa Rock; Skarvsnes; Skallevikhalsen). However, Ti contents of biotite from Rundvågshetta (granulite-facies area) are lower in Ti (0.27 and 0.48 pfu), and have higher X_{Mg} values (0.66–0.74) than other localities (0.49–0.64).

Table 2. Representative electron microprobe results of minerals in mafic metamorphic rocks from the LHC.

Mineral	orthopyroxene						clinopyroxene							Mineral	amphibole					
Analysis No.	44	82	86	89	95	111	38	44	82	86	89	95	111	Analysis No.	38	44	78	89	95	111
Locality	CH	LA	HO	SVN	SVH	RVH	AR	CH	LA	HO	SVN	SVH	RVH	Locality	AR	CH	AP	SVN	SVH	RVH
SiO_2	53.10	52.33	52.53	52.92	51.57	53.26	53.46	53.04	52.74	52.51	52.69	51.65	52.99	SiO_2	43.71	44.34	43.04	42.63	42.99	45.62
TiO_2	0.00	0.06	0.16	0.07	0.12	0.12	0.20	0.23	0.23	0.31	0.22	0.27	0.14	TiO_2	1.03	1.56	2.12	2.52	2.50	2.06
Al_2O_3	0.97	0.88	0.86	1.00	1.34	0.49	1.41	1.96	1.69	1.71	1.97	2.65	1.55	Al_2O_3	12.18	11.70	10.93	10.85	11.33	9.00
Cr_2O_3	0.00	0.02	0.06	0.05	0.10	0.01	0.00	0.00	0.00	0.02	0.09	0.12	0.17	Cr_2O_3	0.03	0.00	0.03	0.13	0.36	0.21
FeO*	25.79	29.75	27.98	25.29	29.35	26.08	8.26	12.16	11.61	10.59	9.56	11.42	10.79	FeO*	15.94	14.82	17.44	14.40	17.29	15.31
MnO	1.08	0.49	0.52	0.67	0.64	0.73	0.43	0.35	0.08	0.23	0.38	0.30	0.30	MnO	0.53	0.22	0.38	0.14	0.25	0.23
MgO	19.91	17.44	18.17	19.52	18.12	19.81	12.82	13.25	12.04	12.70	13.02	11.99	12.92	MgO	10.54	11.54	10.66	11.35	10.32	12.46
CaO	0.46	0.60	0.82	0.61	0.67	0.77	23.78	20.44	21.78	21.74	21.93	21.25	21.46	CaO	12.08	11.58	11.63	11.37	11.38	11.14
Na_2O	0.01	0.05	0.06	0.02	0.01	0.00	0.59	0.43	0.29	0.28	0.43	0.46	0.89	Na_2O	1.24	1.42	1.95	1.45	1.68	1.96
K_2O	0.00	0.02	0.01	0.01	0.00	0.01	0.00	0.01	0.00	0.00	0.02	0.00	0.01	K_2O	1.55	1.40	0.86	1.58	1.38	1.25
Total	101.34	101.64	101.16	100.16	101.91	101.28	100.94	101.86	100.46	100.09	100.30	100.11	101.20	Total	98.84	98.57	99.05	96.43	99.48	99.24
Cations (O=6)														Cations (O=23)						
Si	1.984	1.983	1.985	1.994	1.951	1.993	1.978	1.959	1.976	1.968	1.964	1.944	1.969	Si	6.433	6.471	6.335	6.415	6.331	6.638
Ti	0.000	0.002	0.005	0.002	0.003	0.003	0.006	0.006	0.007	0.009	0.006	0.008	0.004	Ti	0.114	0.171	0.234	0.285	0.277	0.226
Al	0.043	0.039	0.038	0.044	0.060	0.022	0.061	0.085	0.075	0.076	0.087	0.117	0.068	Al	2.112	2.013	1.897	1.925	1.966	1.543
Cr	0.000	0.001	0.002	0.002	0.003	0.000	0.000	0.000	0.000	0.001	0.003	0.004	0.005	Cr	0.003	0.000	0.003	0.016	0.042	0.024
Fe	0.806	0.943	0.884	0.797	0.928	0.816	0.256	0.376	0.364	0.332	0.298	0.359	0.335	Fe^{2+}	1.624	1.389	1.569	1.528	1.641	1.391
Mn	0.034	0.016	0.016	0.021	0.021	0.023	0.013	0.011	0.002	0.007	0.012	0.009	0.009	Fe^{3+}	0.338	0.420	0.578	0.284	0.488	0.472
Mg	1.109	0.985	1.024	1.096	1.022	1.105	0.707	0.729	0.672	0.709	0.723	0.673	0.715	Mn	0.066	0.027	0.048	0.018	0.031	0.028
Ca	0.018	0.024	0.033	0.025	0.027	0.031	0.943	0.809	0.874	0.873	0.876	0.857	0.854	Mg	2.312	2.510	2.339	2.546	2.266	2.702
Na	0.001	0.004	0.004	0.002	0.000	0.000	0.042	0.031	0.021	0.020	0.031	0.034	0.064	Ca	1.904	1.811	1.835	1.833	1.795	1.737
K	0.000	0.001	0.000	0.000	0.000	0.001	0.000	0.000	0.000	0.000	0.001	0.000	0.000	Na	0.259	0.213	0.391	0.256	0.275	0.290
														K	0.292	0.260	0.161	0.304	0.260	0.232
Total	3.995	3.998	3.992	3.982	4.015	3.993	4.007	4.007	3.991	3.995	4.001	4.005	4.023	Total	15.458	15.285	15.390	15.408	15.372	15.283
X_{Mg}	0.58	0.51	0.54	0.58	0.52	0.58	0.73	0.66	0.65	0.68	0.71	0.65	0.68	Mg/(Mg +Fe^{2+})	0.59	0.64	0.60	0.62	0.58	0.66
En	57.37	50.46	52.74	57.16	51.67	56.61	37.12	38.11	35.19	37.05	38.13	35.62	37.55							
Fs	41.68	48.29	45.55	41.55	46.95	41.82	13.41	19.63	19.04	17.34	15.71	19.03	17.61							
Wo	0.95	1.25	1.72	1.28	1.38	1.58	49.47	42.26	45.77	45.60	46.17	45.35	44.84							

*Total Fe as FeO, see Table 1 for analysis No. and locality abbreviations.

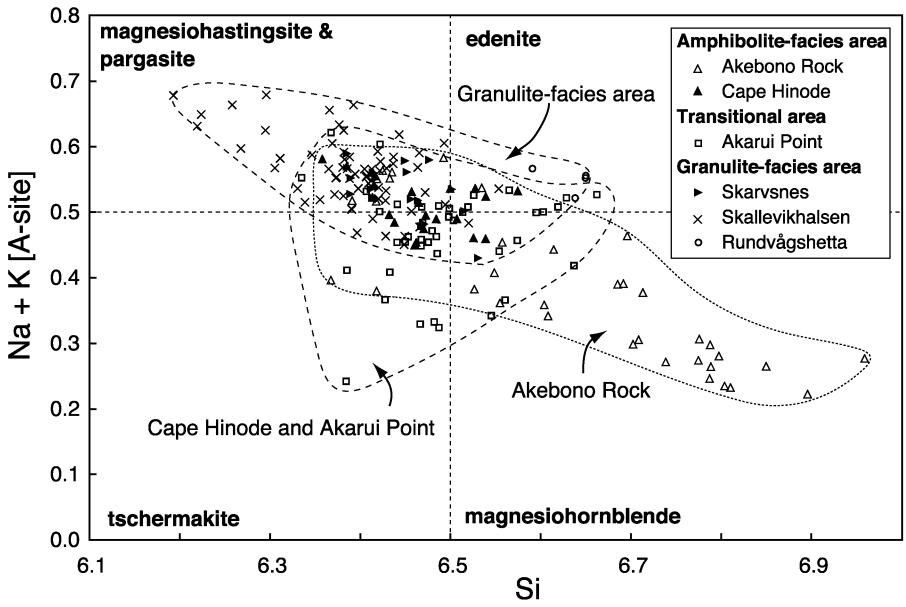

Fig. 4. Classification of calcic amphiboles (Na+K [A-site] versus Si diagram) for the mafic metamorphic rocks from the LHC. Nomenclature and discrimination fields after Leake et al. (1997). Abbreviations are the same as in Table 1.

3.3.5. Plagioclase

Plagioclase grains vary from andesine to bytownite. Plagioclase from Cape Hinode, Langhovde, Honnör Oku-iwa Rock, Skarvsnes and Skallevikhalsen has higher anorthite (An: $CaAl_2Si_2O_8$) contents (40–86%) than those from Akebono Rock and Akarui Point (26–47%). Plagioclase from Rundvågshetta has lower An content (20–25%). Motoyoshi (1986) indicated that Na contents of plagioclase in this area relate to Na content in clinopyroxene (0.05–0.07 pfu versus 0.02–0.05 pfu in other localities). It has been suggested that amphibole breakdown during decompression released Na, which was distributed between clinopyroxene and plagioclase. Chemical zoning is found in some plagioclase, where An decreases from core to rim.

3.3.6. Garnet

Garnet occurs in mafic metamorphic rocks from the transitional area and granulite-facies area. In this study, two grains of garnet from Rundvågshetta were analyzed. Composition ranges from $Pyr_{16-19}Alm_{58-61}Sps_{3-4}Grs_{18-22}$ in rims to $Pyr_{17-20}Alm_{57-61}Sps_{3-5}Grs_{18-21}$ in cores. The X_{Mg} values range between 0.21 and 0.24 in rims, and 0.22 and 0.26 in cores.

3.3.7. Accessory minerals

Epidote is found in amphibolite from Akebono Rock, as needles included in plagioclase (Ab_{53-64}) and amphibole. The X_{Fe} ($Fe^{3+}/(Fe^{3+}+Al)$) values of epidote range between 0.15 and 0.20. Opaque minerals are Fe-Ti oxides or sulphides. The Fe-Ti oxides vary from ilmenite through hematite to magnetite. Ilmenite with magnetite is found in samples from Akebono Rock and Cape Akarui. Ilmenite with hematite

exsolution lamellae is found in samples from Skallevikhalsen. Pyrite is found in samples from Akebono Rock, Akarui Point and Skallevikhalsen.

3.4. Summary of petrography

Textural features of minerals comprising mafic metamorphic rocks are of completely recrystallised textures, such as retrogressive mineral reactions around garnet and clinopyroxene, polygonal aggregates of plagioclase, pyroxenes, hornblende and biotite; and strongly aligned aggregates of hornblende and biotite are found. Metamorphic areas along the LHC reflect compositions of minerals of these recrystallised textures. Ti (pfu) contents of hornblende vary from 0.04 to 0.25 in the amphibolite-facies area and 0.21 to 0.30 in transitional granulite and granulite-facies areas, indicating amphibolite-facies and up to granulite-facies metamorphic conditions, respectively (Raase, 1974). On the basis of a discrimination diagram by Rietmeijer (1983), compositions of orthopyroxene coexisting with Ca-rich clinopyroxene are grouped into metamorphic orthopyroxenes (*i.e.*, ratio of $100\times Ca/(Fe^{2+}+Mg+Ca)$ is 0.95–0.72 at a ratio of $Fe^{2+}/(Fe^{2+}+Mg)$ is 0.42–0.49; Fe^{2+} are estimated from the method by Droop, 1987). Thus, textural features and compositions of minerals are typical metamorphic and no magmatic relics are preserved.

4. Whole-rock geochemistry

4.1. Analytical method

A total of 53 samples were analyzed for major elements as oxides and trace elements (Co, Cr, Cu, Nb, Ni, Rb, Sr, V, Y, Zn and Zr) using the X-ray fluorescence spectrometer (XRF: Rigaku RIX3000) at the National Institute of Polar Research (NIPR), Tokyo, Japan. Analytical conditions and methods follow Motoyoshi and Shiraishi (1994) and Motoyoshi *et al.* (1996), where the contents of H_2O^+ and H_2O^- are included into the total weight percent of major oxides. The rocks analyzed in this study include intermediate orthogneiss (*i.e.*, 52–62 wt% SiO_2) and mafic orthogneiss (*i.e.*, 45–52 wt% SiO_2). Representative results of the whole-rock compositions are listed in Table 3. Precisions evaluating from values of geochemical reference samples (GSJ Japan: JA-2, JB-1a, JB-3 and JGb-1) were $<5\%$ for major elements, V, Zn, Rb, Sr and Zr, $<10\%$ for Cr and Nb, $<15\%$ for Co and Ni, and 15–25% relatively low for Y.

4.2. Chemical alteration

On a geochemical basis, mafic metamorphic rocks are generally thought to have derived from igneous protoliths such as basalt and gabbro (*e.g.*, Bucher and Frey, 1994). However, in order to recover protolith compositions, we must take into account the effects of metamorphic processes on bulk composition, especially partial melting, allochemical metamorphism, solid state diffusion controlled by temperature, fluid-induced metasomatism, weathering and seawater alteration (*e.g.*, Rollinson, 1993; Shuto and Osanai, 2002). Many previous workers have concluded that large ion lithophile elements (LILE) are relatively mobile, whereas high field strength elements (HFSE) are relatively immobile during metamorphism (*e.g.*, Chocyk-Jaminski and Dietsch, 2002; Khan *et al.*, 2005).

Table 3. Representative whole-rock compositions of mafic metamorphic rocks analyzed in this study from the LHC.

Analysis No.	3	7	32	33	35	36	38	40	44	10	11	76	78	79	82	86	87	88
Locality	AR	AR	AR	AR	AR	AR	AR	CH	CH	AP	AP	AP	AP	AP	LA	HO	SVN	SVN
Major elements (wt%)																		
SiO_2	51.30	51.69	50.68	49.67	48.73	50.70	51.08	47.55	51.40	50.61	49.96	50.76	50.40	47.50	46.78	48.31	46.13	45.32
TiO_2	1.01	0.79	1.02	0.75	0.81	0.79	0.86	0.45	0.64	1.00	2.02	1.03	1.23	1.10	3.79	1.78	0.54	0.52
Al_2O_3	14.53	15.29	14.52	15.84	15.67	15.30	18.13	18.16	16.49	15.64	15.23	15.23	14.69	15.42	14.91	15.95	13.73	14.01
$Fe_2O_3^t$	15.32	11.55	15.22	12.13	11.57	10.15	8.90	7.63	9.71	11.12	12.65	10.61	10.93	11.02	15.11	13.19	10.63	10.58
MnO	0.26	0.19	0.25	0.23	0.28	0.25	0.17	0.17	0.17	0.15	0.17	0.20	0.21	0.25	0.15	0.18	0.15	0.16
MgO	4.80	7.28	5.14	7.46	8.76	8.20	5.50	9.29	6.85	7.47	6.56	7.45	6.93	7.69	6.26	7.36	17.56	16.65
CaO	8.72	11.00	8.79	9.49	8.83	10.63	10.61	14.34	10.35	9.80	6.00	10.58	11.14	12.28	8.72	9.47	8.79	9.36
Na_2O	3.85	2.84	3.99	3.53	3.22	3.27	3.98	2.25	3.83	3.31	3.65	3.28	3.53	3.37	1.52	1.90	1.52	1.91
K_2O	0.13	0.24	0.31	0.85	1.95	0.85	0.91	0.62	0.87	0.62	2.91	0.82	0.55	1.14	1.51	1.17	0.55	0.85
P_2O_5	0.11	0.08	0.09	0.09	0.04	0.05	0.09	0.07	0.07	0.12	0.44	0.11	0.24	0.11	0.75	0.36	0.13	0.08
total	100.04	100.94	100.01	100.03	99.85	100.19	100.23	100.52	100.36	99.83	99.58	100.06	99.85	99.87	99.49	99.69	99.71	99.43
Trace elements (ppm)																		
Co	52.9	55.2	44.4	40.8	39.4	36.4	30.0	31.4	34.4	37.4	35.7	37.4	38.1	38.0	43.5	45.9	58.2	60.6
Cr	8.4	129	17.5	221	204	204	79.9	139	79.6	234	9.4	253	180	234	101	131	1069	1042
Cu	10.9	57.6	7.1	1.7	lld	lld	12.6	6.9	lld	29.8	18.8	56.7	56.7	6.3	30.5	24.0	63.6	7.2
Nb	lld	lld	2.9	2.8	2.3	4.1	3.9	3.8	2.1	7.0	5.2	4.2	4.6	2.0	14.2	7.2	2.9	3.3
Ni	7.6	48.5	8.3	52.7	84.1	78.0	26.3	42.5	33.8	93.9	5.9	74.1	55.8	103	39.2	60.6	416	70.1
Rb	9.2	2.1	2.2	11.5	65.6	7.0	7.3	2.1	4.0	9.7	82.1	7.6	9.9	7.2	137	19.1	8.4	20.7
Sr	235	185	219	150	156	171	238	331	170	233	290	218	331	246	39.8	266	299	187
V	470	304	494	334	236	221	221	157	233	210	336	236	264	268	187	204	120	113
Y	15.4	18.9	15.8	13.9	18.8	17.9	20.5	11.5	13.8	29.8	34.8	22.8	27.5	20.8	50.0	31.3	10.2	10.5
Zn	96.8	76.2	109	88.9	116	94.8	62.3	65.5	67.4	131	106	86.3	93.3	124	166	106	86.7	108
Zr	32.7	35.5	30.9	30.0	35.9	36.6	59.8	39.3	34.8	77.3	123	101	81.9	55.4	343	179	57.7	53.4

Analysis No.	89	14	92	93	94	95	96	100	101	102	103	105	108	16	17	109	110	111
Locality	SVN	SVH	SVH	SVH	SVH	SVH	SVH	SVH	SVH	SVH	SVH	SVH	SVH	SVH	SVH	RVH	RVH	RVH
Major elements (wt%)																		
SiO_2	48.14	46.57	48.32	47.30	46.87	47.73	48.90	45.57	45.01	47.01	47.61	46.88	45.43	48.56	49.72	48.89	49.92	50.99
TiO_2	1.97	1.18	1.00	1.53	1.13	1.19	1.28	3.49	3.45	1.76	0.91	1.50	2.85	1.06	1.00	1.01	0.42	1.40
Al_2O_3	15.19	13.33	13.85	12.76	13.42	11.70	14.12	14.46	14.94	15.59	13.67	13.68	14.94	7.16	7.47	7.18	9.09	10.39
$Fe_2O_3^t$	11.98	15.59	13.62	16.47	15.44	14.93	12.31	16.45	16.50	13.01	14.16	14.26	15.32	14.09	13.79	14.19	12.00	15.28
MnO	0.15	0.25	0.20	0.23	0.23	0.24	0.18	0.23	0.22	0.18	0.24	0.25	0.24	0.20	0.22	0.24	0.21	0.26
MgO	7.98	7.71	8.15	7.11	7.76	9.35	7.86	6.00	5.02	7.39	7.96	7.74	6.82	15.60	14.65	14.36	16.22	8.55
CaO	8.82	13.35	12.80	12.29	12.98	12.93	12.19	8.76	8.78	9.49	12.88	12.66	9.31	7.61	7.65	7.66	9.16	8.86
Na_2O	2.73	1.52	1.26	1.44	1.62	1.34	2.13	3.02	3.06	3.16	1.44	2.37	3.03	1.17	1.53	1.54	1.90	3.48
K_2O	2.55	0.42	0.75	0.57	0.46	0.31	0.80	1.01	1.79	1.84	0.47	0.94	1.62	3.50	3.10	3.10	1.04	0.79
P_2O_5	0.28	0.09	0.07	0.10	0.09	0.09	0.11	0.47	0.45	0.15	0.06	0.11	0.34	0.21	0.19	0.21	0.04	0.28
total	99.79	100.01	100.02	99.79	99.98	99.79	99.88	99.46	99.20	99.58	99.39	100.41	99.89	99.15	99.33	98.38	99.99	100.29
Trace elements (ppm)																		
Co	40.3	47.9	47.2	51.9	53.4	49.3	42.4	48.4	46.0	42.4	45.0	42.1	46.5	54.1	51.6	51.9	50.6	54.8
Cr	278	105	181	127	102	786	245	105	74.9	125	199	106	136	792	762	743	1360	457
Cu	60.2	140	169	239	199	115	150	92.4	103	36.2	70.9	98.7	138	8.1	5.6	17.3	lld	39.5
Nb	6.8	4.1	3.9	5.0	5.0	4.7	7.3	14.6	8.6	4.7	2.5	6.0	10.7	8.8	10.4	12.0	4.5	16.7
Ni	87.8	55.9	80.7	64.5	58.0	88.0	99.8	71.7	48.6	95.6	58.6	73.8	73.9	588	533	524	247	185
Rb	101	4.8	15.5	7.2	lld	3.9	8.0	14.9	56.8	67.1	4.1	16.7	35.8	312	323	340	32.1	7.6
Sr	286	115	133	110	121	87	164	291	263	284	118	186	219	139	110	154	123	371
V	193	366	331	417	356	389	308	239	258	247	340	380	264	203	188	238	185	273
Y	30.0	23.2	19.0	26.5	21.5	26.5	24.2	40.3	44.6	25.2	19.3	23.9	40.5	25.9	26.6	26.8	10.5	38.2
Zn	128	96.9	94.5	100	99.5	107	91.1	129	172	138	87.9	138	125	115	138	148	103	135
Zr	136	50.9	44.4	67.4	48.9	50.0	90.0	244	218	84.8	34.0	72.0	191	97.2	97.7	99.1	25.6	90.8

$Fe_2O_3^t$ as total iron, lld; lower than detection limit, see Table 1 for analysis No. and locality abbreviations.

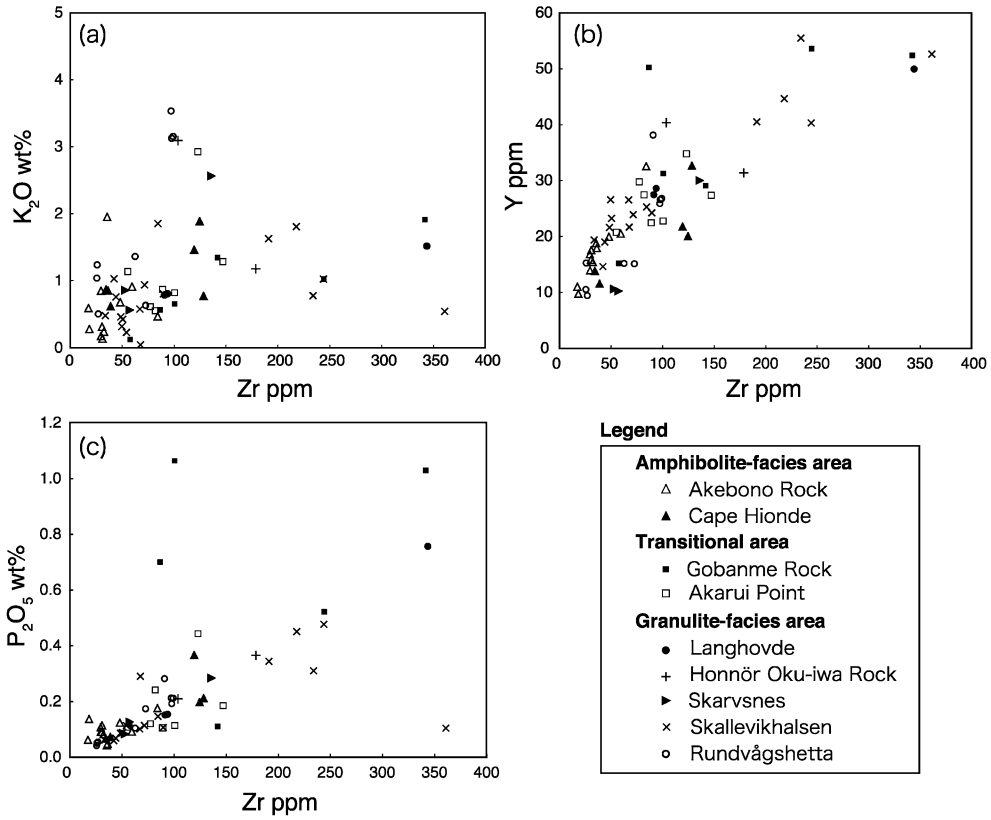

Fig. 5. Diagrams showing variations of K_2O (a), Y (b) and P_2O_5 (c) contents with respect to Zr contents for the mafic and intermediate metamorphic rocks analyzed in this study.

On the variation diagram, the K_2O contents of the mafic metamorphic rocks in the LHC range between 0.1 and 4.9 wt% (Fig. 5a), whereas K_2O content in basaltic rocks rarely exceeds 2.5 wt% (*e.g.*, Pearce, 1982). The mafic metamorphic rocks are also enriched in Sr and Rb relative to N-type MORB (*e.g.*, Sun and McDonough, 1989). The enrichment of these elements is likely to be a result of hydrothermal alteration during metamorphism, presumably involving seawater in a subduction zone setting (Bebout, 1995). In contrast, the variation diagrams of Y versus Zr (Fig. 5b) and P_2O_5 versus Zr (Fig. 5c) indicate that the majority of the rocks have well-defined positive linear correlations, consistent with compositions commonly observed in igneous suites. From this it can be inferred that the protolithic contents of HFSEs (Y, Ti, Nb and P) are preserved through metamorphism.

4.3. Major elements

Compositions of all the analyzed samples in this and previous studies are plotted on the ACF diagram (Fig. 6). Previous studies include samples from various localities in the LHC. Compositionally, samples from the amphibolite-facies area concentrate in

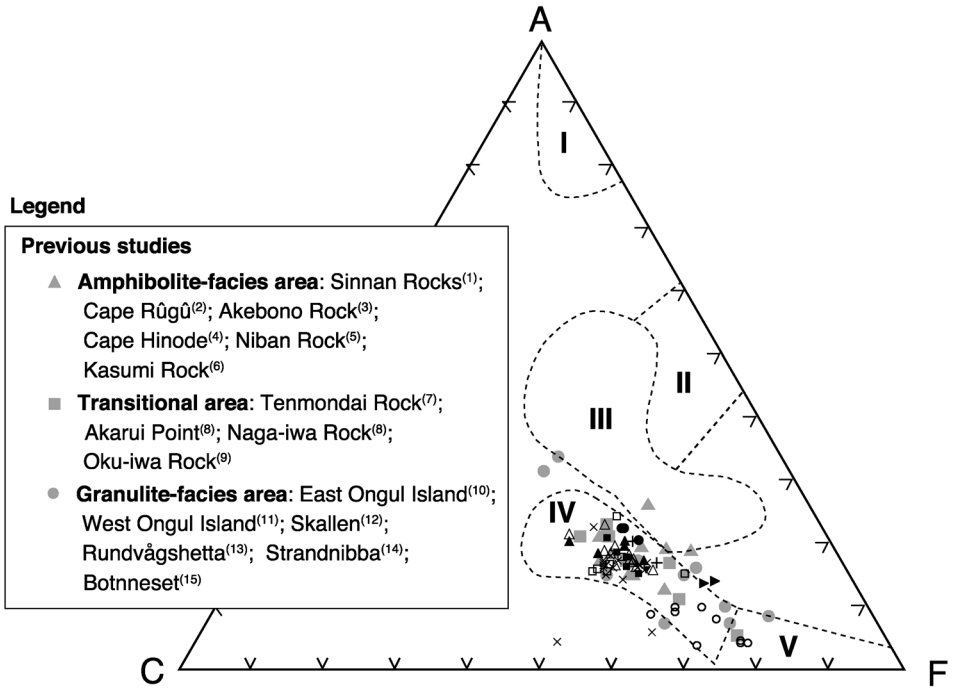

Fig. 6. ACF diagram for the mafic and intermediate metamorphic rocks analyzed in this study and previously. Discrimination fields after Winkler (1979): (I) high-Al mudstone, (II) general mudstone, (III) greywacke, (IV) mafic igneous rock and (V) ultramafic rock. Apexes: A; $Al_2O_3+Fe_2O_3-Na_2O-K_2O$, C; CaO, F; FeO+MnO+MgO. Fe^{3+}/Fe^{total} is assumed to be 0.1. Data sources of the previous studies: (1)Hiroi et al. (1983b); (2)Nakai et al. (1980); (3)Hiroi et al. (1986); (4)Kanisawa et al. (1987); (5)Kizaki et al. (1983); (6)Nishida et al. (1984); (7)Shiraishi et al. (1985); (8)Yanai et al. (1984); (9)Nakai et al. (1981); (10)Yanai et al. (1974a) and Kanisawa et al. (1987); (11)Yanai et al. (1974b), (12)Yoshida et al. (1976) and Osanai et al. (2004); (13)Motoyoshi et al. (1986); (14)Motoyoshi et al. (1985); (15)Shiraishi and Yoshida (1987). Symbols are the same as in Fig. 5.

the basalt and andesite fields, although a few samples from West Ongul Island and East Ongul Island (granulite-facies area) are plotted outside of the field. In contrast, samples from the transitional and granulite-facies areas vary widely from scatter from basalt and andesite to ultramafic rocks in the diagram.

SiO_2 content generally decreases with increasing metamorphic grade, varying from 45–60 wt% in the amphibolite-facies area, through <57 wt% in the transitional area to <53 wt% in the granulite-faces area. $Fe_2O_3{}^t$ and MgO and TiO_2 contents have negative correlations with increasing SiO_2 content (Fig. 7a–c). Al_2O_3 content has an almost constant correlation with increasing SiO_2 content (Fig. 7d). MgO content ranges between 2 and 18 wt%, and can be divided into high-Mg (13–18 wt%) and low-Mg (2–13 wt%) groups (Fig. 7b). High-Mg samples include some rocks of picritic composition (*i.e.*, MgO$>$12 wt%, SiO_2 30–52 wt% and (Na_2O+K_2O) <3 wt%, as defined by Le Bas, 2000). Al_2O_3 content ranges between 2 and 18 wt%, and can be divided into high-Al (12–18 wt%), and low-Al (2–12 wt%) groups (Fig. 7d). All high-Mg samples

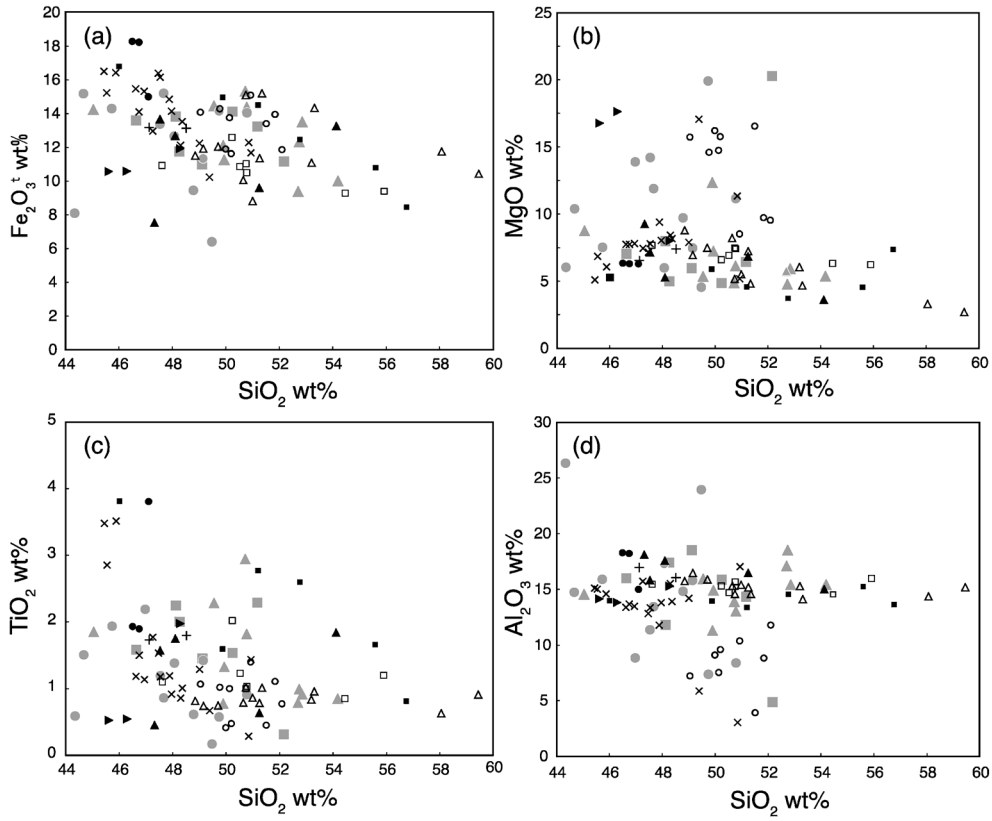

Fig. 7. Harker diagrams showing variations of $Fe_2O_3^t$ (a), MgO (b), TiO_2 (c) and Al_2O_3 (d) contents with respect to SiO_2 contents for the mafic and intermediate metamorphic rocks analyzed in this study and previous studies. Symbols are the same as in Fig. 5 and Fig. 6.

(including the picritic ones) and low-Al samples predominantly occur in the granulite-facies area of the LHC.

On the SiO_2 versus FeO^*/MgO diagram (Fig. 8a) SiO_2 content increases with increasing FeO^*/MgO ratio, indicating tholeiite affinity, although some samples plot in the calc-alkaline field. On the TiO_2 versus FeO^*/MgO variation diagram (Fig. 8b), samples of IAT affinity predominantly occur in the amphibolite-facies area (Sinnan Rocks, Cape Ryûgû, Akebono Rock and Kasumi Rock), with TiO_2 content of around 1.0 wt%. Two samples from Akebono Rock and Kasumi Rock plot in the MORB field. In contrast, samples from transitional and granulite-facies areas have increasing TiO_2 content with increasing FeO^*/MgO ratio, indicating MORB to OIB affinities, with the former being predominant. In addition, some samples from all areas plot in the oceanic plateau basalt (OPB) field, the significance of which will be discussed later.

4.4. Trace elements

Compositions of all analyzed samples in this study are plotted on the diagrams for

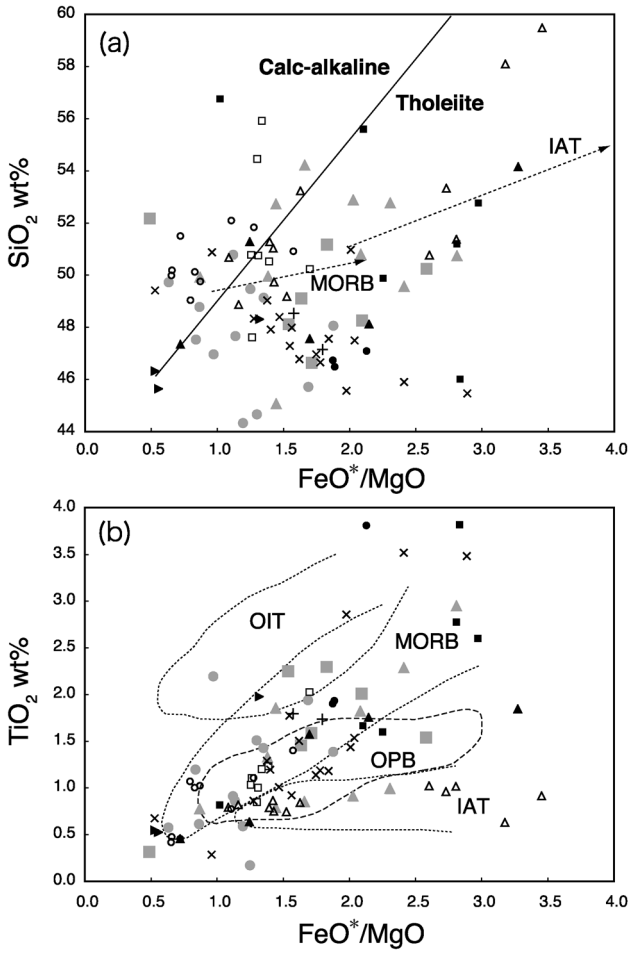

Fig. 8. FeO^*/MgO versus SiO_2 (a) and FeO^*/MgO versus TiO_2 (b) diagrams for the mafic and intermediate metamorphic rocks analyzed in this study and previous studies. Discrimination line between calc-alkaline and tholeiite, and chemical trends of mid-oceanic-ridge basalt (MORB) and island arc tholeiite (IAT) shown by arrows are after Miyashiro (1975). Fields of MORB, IAT and oceanic island basalt (OIB) are after Basaltic Volcanism Study Project (1981). Field of oceanic plateau basalt (OPB) is after Koizumi and Ishiwatari (2006). Symbols are the same as in Fig. 5 and Fig. 6.

distinguishing alkaline and tholeiitic affinities (Winchester and Floyd, 1976; Fig. 9a, b). In these diagrams, the data show a well-defined parallel trend toward increasing Zr/P_2O_5, and increasing Zr content, typical of tholeiitic associations. Relatively low Nb/Y (less than 0.6) is consistent with sub-alkaline affinity (Pearce and Gale, 1977).

The mafic metamorphic rocks analyzed in this study are plotted on discrimination diagrams for basalts from various tectonic settings (Fig. 10). Samples from Akebono Rock predominantly plot in arc-type fields (VAB: volcanic arc basalt, IAB: island arc basalt, and IAT: island arc tholeiite). Samples from other localities (Cape Hinode, Gobanme Rock, Akarui Point, Langhovde, Skarvsnes, Honnör Oku-iwa Rock, Skallevikhalsen and Rundvågshetta) are scattered across all types of basalt, with most samples plotting in the MORB field.

N-type MORB normalized multi-element diagrams (spiderdiagrams) are shown in Fig. 11. All analyzed samples show relative enrichment in LILE (Sr, K and Rb), which may be a result of secondary alteration as previously suggested. Samples from

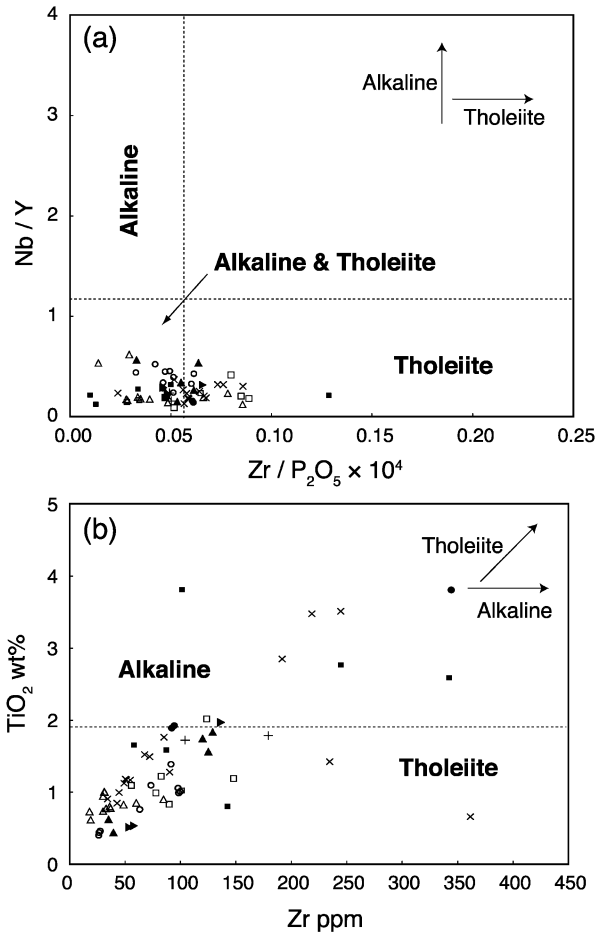

Fig. 9. Nb/Y versus $Zr/P_2O_5 \times 10000$ (a) and TiO_2 versus Zr (b) diagrams for the mafic and intermediate metamorphic rocks analyzed in this study. Discrimination lines and chemical trends (shown by arrows): alkaline (AL) and tholeiite (TH), after Winchester and Floyd (1976). Symbols are the same as in Fig. 5.

Akebono Rock are relatively depleted in HFSEs, and display typical IAT affinities. In contrast, samples from Cape Hinode have HFSE-enriched compositions typical of E-type MORB or OIB affinities. Samples from Skallevikhalsen and Rundvågshetta display both HFSE-depletes and enriched compositions similar to E-type MORB. Samples from other localities (Gobanme Rock, Akarui Point, Langhovde, Honnör Oku-iwa Rocks and Skarvsnes) are relatively enriched in HFSEs, and display trends typical of IAT, N-type and E-type MORB affinities.

In addition to these diagrams, Condie (1999) suggests that Ni content at a given Mg number is a sensitive indicator of the fractionation histories of basalts from various tectonic settings. Subduction-derived basalts have lower Ni content ($<$2 ppm at a Mg# of around 40) than MORB and plume-derived basalts (50–100 ppm). Samples of IAT affinity from Akebono Rock have lower Ni content (7.6–52 ppm) typical of an arc setting, whereas samples from transitional and granulite-facies localities have higher Ni content (56–185 ppm) typical of MORB or plume-derived basalt affinities.

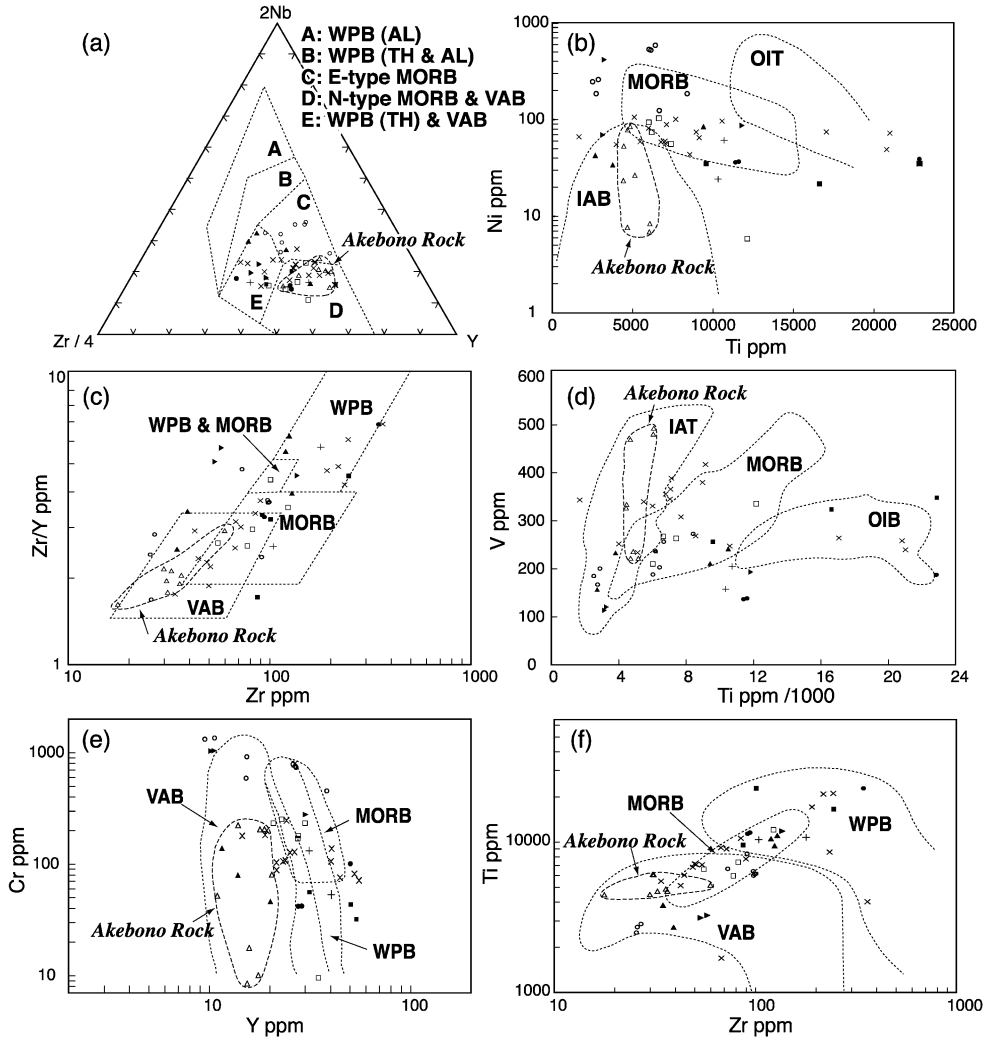

Fig. 10. Diagrams showing compositional fields of basalts in various tectonic settings and compositional variations of the mafic metamorphic rocks analyzed in this study. Discrimination fields: (a) after Meschede (1986); (b) after Ishizuka (1981); (c) after Pearce and Norry (1979); (d) after Shervais (1982); (e) after Pearce (1982); (f) after Pearce (1982). Abbreviations: WPB; within-plate basalt, OIT; oceanic island tholeiite, OIB; oceanic island basalt, VAB; volcanic arc basalt, IAT; island arc tholeiite, IAB; island arc basalt, AL; alkaline, TH, tholeiite. Symbols are the same as in Fig. 5.

5. Discussion

5.1. Tectonic setting for protoliths of mafic metamorphic rocks

Major and trace element bulk-rock compositions analyzed in this and previous studies indicate that rocks of IAT and MORB affinities occur in amphibolite-facies localities (excluding Cape Hinode), with rocks of IAT affinity predominantly in the SW

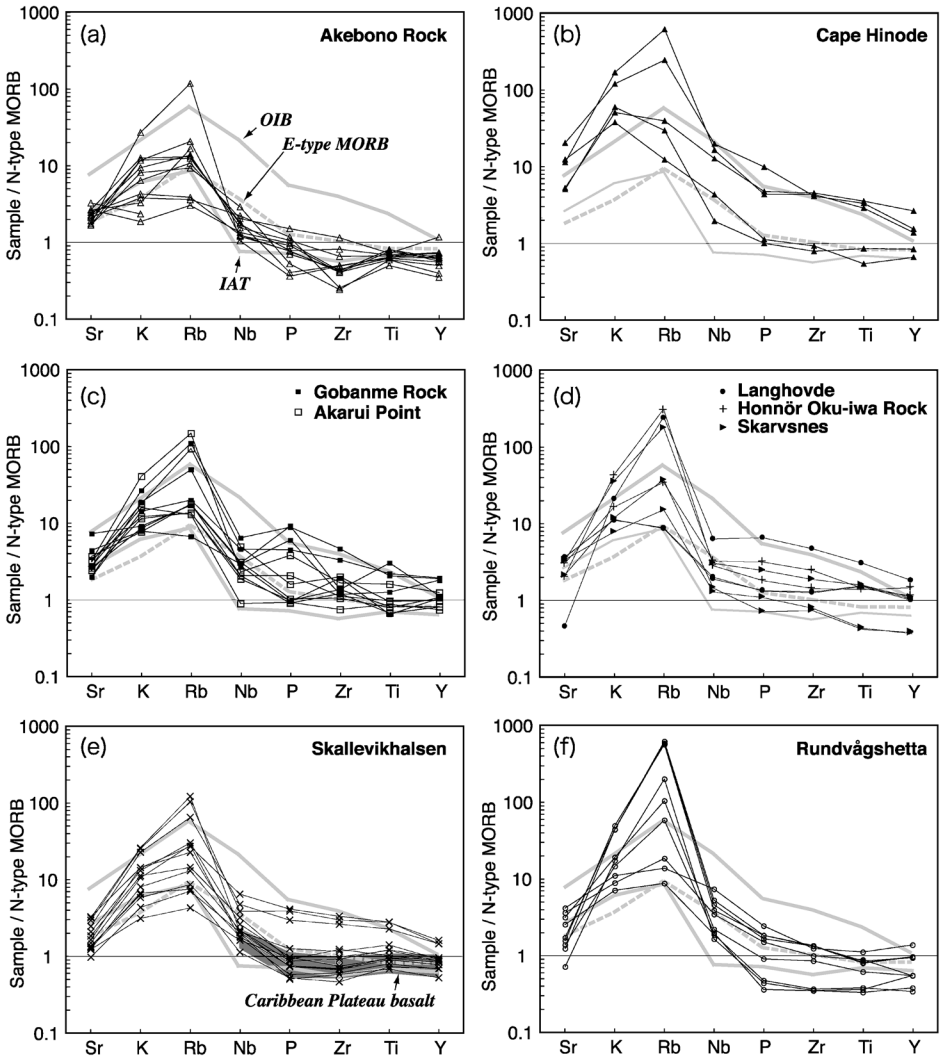

Fig. 11. N-type MORB normalized multi-element diagrams (spiderdiagrams) for the mafic and intermediate metamorphic rocks analyzed in this study from Akebono Rock (a), Cape Hinode (b), Akarui Point and Gobanme Rock (c), Langhovde, Honnör Oku-iwa Rock and Skarvsnes (d), Skallevikhalsen (e) and Rundvågshetta (f). Values of N-type MORB, oceanic island basalts (OIB) and E-type MORB are after Sun and McDonough (1989). Caribbean Plateau basalt (shown by gray field) is after Nagahashi and Miyashita (2002).

end of the amphibolite-facies zone (Sinnan Rock, Cape Ryûgû and Akebono Rock). Rocks with IAT and MORB affinities also occur in the transitional granulite and granulite-facies areas, but are less abundant than those with MORB affinities. The results indicate that mafic protoliths in the LHC shift from IAB to MORB affinities from NE to SW and with increasing metamorphic grade. Rocks from Cape Hinode are

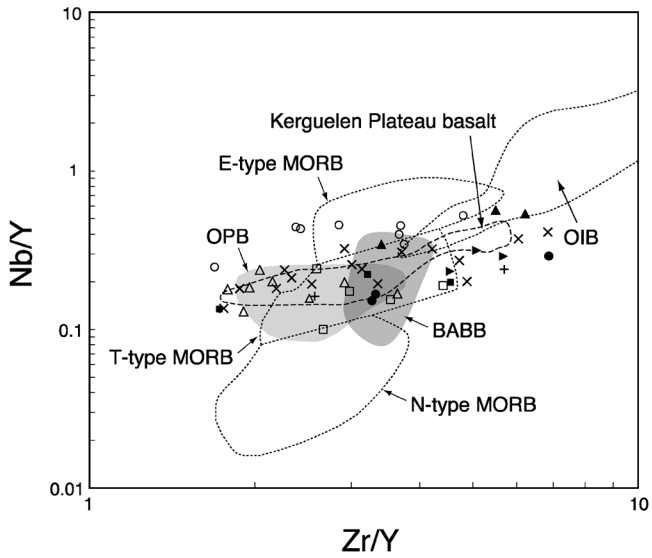

Fig. 12. Nb/Y versus Zr/Y diagram for the mafic metamorphic rocks analyzed in this study. Fields of oceanic island basalts (OIB), N-type MORB, T-type MORB and E-type MORB are after Ueda et al. (2000), oceanic plateau basalts (OPB) is after Koizumi and Ishiwatari (2006), Kerguelen Plateau basalt is after Storey et al. (1992), back arc basin basalt (BABB) is after Kerr et al. (2000). Symbols and data sources are the same as in Fig. 5.

indistinguishable on geochemistries, in which they show trace element patterns similar to E-type MORB and OIB in the spiderdiagram (Fig. 11b); in contrast, they are mostly plotted in the field of VAB or IAT on the discrimination diagrams (Fig. 10).

Field relationships suggest that rocks of IAT affinity at Akebono Rock (amphibolite-facies area) may have intruded into pelitic rocks. In contrast, rocks of MORB or IAT affinities do not preserve pre-metamorphic relationships, and may have been juxtaposed with metasediments by intrusive, extrusive or accretionary processes. Geological relationships between rocks of IAT and MORB affinities have not been observed. Blocks of ultramafic rocks, which may have originated as remnants of oceanic crust, predominantly occur in the central and SW parts of the LHC (*e.g.*, Hiroi *et al.*, 1986). The SiO_2 content of the mafic metamorphic rocks increases from SW to NE, tending towards andesitic composition. It is possible that this distribution represents differences in tectonic settings of the protoliths between localities.

Further inferences about the tectonic setting of mafic protoliths can be made from the Nb/Y versus Zr/Y diagram in Fig. 12 (Ueda *et al.*, 2000). Samples of MORB affinity in the transitional and granulite-facies areas have E-type MORB and T-type MORB affinities, in which samples from Rundvågshetta have higher Nb/Y ratios (0.25–0.5) than those from other occurrences (0.1–0.41). Samples of IAT affinity from Akebono Rock have already been distinguished from MORB affinities, as discussed above.

5.1.1. Possible presence of oceanic plateau basalt (OPB)

Oceanic plateau basalt (OPB) and back arc basin basalt (BABB) cannot be distinguished from T-type MORB by Nb/Y ratios. Other methods, however, are available to detect their presence. OPBs have lower Ti and P contents and higher Nb content than N-type MORB (Nagahashi and Miyashita, 2002). The spiderdiagrams indicate that such rocks occur in Skallevikhalsen (Fig. 11e), and display HFSE patterns resembling OPB (Caribbean Plateau basalt), although some samples also plot outside the OPB field (Fig. 8b; Fig. 12). Samples from other localities are relatively enriched and/or depleted in HFSE compared to N-type MORB, and they are plotted inside and/or outside the OPB field in the variation diagrams (Fig. 8b; Fig. 12). These compositions possibly reflect a variety of protolith compositions. However, these compositions bear comparison with basalts of the Kerguelen Plateau, which was generated along the continental margin of India–Australia–Antarctica and involved subcontinental lithospheric mantle and/or continental crust (Storey *et al*., 1992). Kerguelen Plateau basalts have progressively depleted compositions resembling T-type and E-type MORB on the Spiderdiagram; however they can be distinguished from these types by wide compositional variations on various diagrams (Fig. 8b; Fig. 12). Geochemical characteristics of the rocks from the transitional and granulite-facies areas are broadly similar to Kerguelen Plateau basalts. The possibility of oceanic plateau involvement is supported by occurrences of high-Mg basalt, including picrite and komatiite (Kerr *et al*., 2000), in the granulite zone of the LHC. However, it is also possible that the high-Mg mafic rocks represent refractory materials generated by deep crustal anatexis.

5.1.2. Possible presence of back arc basin basalts (BABB)

Field occurrences indicate that mafic metamorphic rocks are closely associated with metasedimentary lithologies. The association of mafic magmatism with abundant amounts of chemically immature sediment is consistent with a coastal continental or evolved island setting for deposition of mafic protoliths. Further, it is well known that basaltic rocks of marginal basins are enriched in incompatible elements relative to N-type MORB (*e.g*., Ishiwatari *et al*., 1991). Kerr *et al.* (2000) suggest that OPBs have higher Ni content than BABBs at a given Mg number. Ni contents of samples from the transitional and granulite-facies areas average at around 80 for Mg numbers of about 40, and are consistent with both BABB and OPB.

5.2. Geological significance of mafic metamorphic rocks in the LHC

On the basis of trace element geochemistry, the mafic metamorphic rocks from the transitional granulite and granulite-facies areas have been classified into enriched MORB affinities, including T-type MORB and E-type MORB. Rocks of E-type MORB affinity predominantly occur in the Rundvågshetta, and may have been generated by mantle plume activity. Rocks of T-type MORB affinity are more widespread and have both BABB and OPB affinities. Moreover, the mafic metamorphic rocks in these areas are closely associated with metasedimentary rocks, suggesting eruption and sedimentation in a marginal sea setting. Some marginal basins (*e.g*., Black Sea; Yamato basin) have thickened oceanic crust, in which T-type MORBs erupted (*e.g*., Ishiwatari *et al*., 1991). These results suggest that mafic metamorphic rocks of T-type and E-type MORB affinities originally formed as a basement of a marginal sea basin more or less affected by hot plume activity, comparable to greenstone terranes in

accretionary complexes, such as the Permian Yakuno Ophiolite (Ishiwatari *et al*., 1991; Ichiyama and Ishiwatari, 2004) or the Jurassic Tamba accretionary complex (Koizumi and Ishiwatari, 2006) in southwest Japan.

The Lützow-Holm Complex (LHC), located in the eastern DML area, is a key area for investigations of reconstruction of the Gondwana supercontinent. The Mozambique Belt is an orogenic belt formed as a result of a final collision between East Gondwana and West Gondwana during the Pan-African (*ca.* 530 Ma). The Mozambique Belt extends from Eastern Africa through India and Sri Lanka to Dronning Maud Land (DML) in East Antarctica (*e.g*., Stern, 1994; Shiraishi *et al*., 1994; Jacobs *et al*., 1998; Jacobs and Thomas, 2004). Many authors have argued that the DML represents a southern extension of the suture between East Gondwana and West Gondwana (*e.g*., Shiraishi *et al*., 1994; Grunow *et al*., 1996; Wilson *et al*., 1997; Kriegsman, 1995; Carson *et al*., 1996; Fitzsimons, 1996, 2000; Hensen and Zhou, 1997). Intercontinental sutures are generally characterized by occurrences of high-grade metamorphic rocks and a mixture of crustal materials, including oceanic, island arc, oceanic island, and oceanic plateau crust and accreted sediments. Such remnants are observed in many parts of the Mozambique Belt and related intercontinental sutures (*e.g*., Osanai *et al*., 1992; Meert, 2003; Kehelpannala, 2004).

Petrographic and geochemical results in this study indicate that mafic metamorphic rocks in the NE part of the LHC (amphibolite-facies area) originated as arc components, whereas mafic metamorphic rocks in the central and SW parts of the LHC (transitional and granulite-facies areas) seem to have mostly originated as oceanic components. In previous studies, the Lützow-Holm Bay area (granulite-facies area) was divided into three groups on the basis of lithostratigraphy and rock constituents (*e.g*., Yoshida, 1978): charnockitic gneiss with quartzo-feldspathic gneiss and marble (Skallen Group), charnockitic gneiss with garnet-biotite gneiss (Ongul Group) and pink granite with biotite gneiss (Okuiwa Group). This variety of lithologies shows that the LHC is composed of various elements of both oceanic crust and island arc crust, with a complex history of sedimentation and igneous activity under an evolving tectonic setting.

6. Conclusions

1) The mode of occurrence of mafic metamorphic rocks changes with increasing metamorphic grade from NE to SW in the LHC. On the basis of field relationships, rocks in the NE part (amphibolite-facies area: Akebono Rock) may have intruded into pelitic rocks. Rocks from the central and SW parts (transitional granulite and granulite-facies areas) may have originated as accreted blocks, magmatic intrusions or volcanics prior to high-grade metamorphism and deformation. On the basis of whole-rock geochemistry, in the NE area, mafic metamorphic rocks of IAT affinity are predominant. In the central and SW parts, rocks of MORB affinity predominate.

2) On the basis of HFSE contents, Nb/Y and Zr/Y ratios, MORB-type compositions have E-type MORB and T-type MORB affinities. In addition, they show both OPB and BABB affinities. Field relationships indicate that mafic protoliths formed in a marginal sea basin setting. Arc components comprise the metamorphic rocks in the

NE part of the LHC, whereas the components of marginal sea basin including OPB and BABB comprise the metamorphic rocks in the central and SW parts of the LHC.

Acknowledgments

We express our sincere thanks to all members of JARE-46 (2004–2006) and the crew of the icebreaker "*Shirase*" for their support during our field operation. Thanks are also due to Prof. Y. Osanai, Prof. K. Shiraishi and Dr. N. Ishikawa for their support on the expedition in Antarctica. We would also like to extend special thanks to Dr. T. Hokada, Dr. D.J. Dunkley, Prof. H. Ishizuka and Dr. M. Owada for helpful discussions and comments, and K. Seno for technical assistance in the XRF analysis. MS-K acknowledges assistance from a JSPS grant-in-aid (No. 15740302).

References

Basaltic Volcanism Study Project (1981): Basaltic Volcanism on the Terrestrial Planets. New York, Pergamon Press, 1286 p.

Bebout, G.E. (1995): The impact of subduction-zone metamorphism on mantle-ocean chemical cycling. Chem. Geol., **126**, 191–218.

Bucher, K. and Frey, M. (1994): Petrogenesis of Metamorphic Rocks. New York, Springer, 318 p.

Carson, C.J., Fanning, C.M. and Wilson, C.J.L. (1996): Timing of the progress granite, Larsemann Hills: additional evidence for Early Palaeozoic orogenesis within the East Antarctic Shield and implication for Gondwana assembly. Aust. J. Earth. Sci., **43**, 539–553.

Chocyk-Jaminski, M. and Dietsch, C. (2002): Geochemical and tectonic setting of metabasic rocks of the Gneiss Dome Belt, SW New England Appalachians. Phys. Chem. Earth, **27**, 149–167.

Condie, K.C. (1999): Mafic crustal xenoliths and the origin of the lower continental crust. Lithos, **46**, 95–101.

Droop, G.T.R. (1987): A general equation for estimating Fe^{3+} concentrations in ferromagnesian silicates and oxides using stoichiometric criteria. Mineral. Mag., **51**, 431–435.

Fitzsimons, I.C.W. (1996): Metapelitic migmatites from Brattstrand Bluffs, East Antarctica—metamorphism, melting and exhumation of the mid crust. J. Petrol., **37**, 395–414.

Fitzsimons, I.C.W. (2000): A review of tectonic events in the East Antarctic Shield and their implications for Gondwana and earlier super continents. J. Afr. Earth Sci., **31**, 3–23.

Fraser, G.L. (1997): Geochronological constraints on the metamorphic evolution and exhumation of the Lützow-Holm Complex, East Antarctica. Ph.D. Thesis, Australian National University, 254 p.

Fraser, G.L., McDougall, I., Ellis, D.J. and Williams, I.S. (2000): Timing and rate of isothermal decompression in Pan-African granulites from Rundvågshetta, East Antarctica. J. Metamorph. Geol., **18**, 441–454.

Grunow, A., Hanson, R. and Wilson, T. (1996): Were aspect of Pan-African deformation linked to lapetus opening? Geology, **24**, 1063–1066.

Hensen, B.J. and Zhou, B. (1997): East Gondwana amalgamation by Pan-African collision? Evidence from Prydz Bay, East Antarctica. The Antarctic Region: Geological Evolution and Processes, ed. by C.A. Ricci. Siena, Terra Antarct. Publ., 115–119.

Hiroi, Y., Shiraishi, K., Yanai, K. and Kizaki, K. (1983a): Geology and petrology of Prince Olav Coasts, East Antarctica. Antarctic Earth Science, ed. by R.L. Oliver *et al.* Canberra, Aust. Acad. Sci., 32–35.

Hiroi, Y., Shiraishi, K. and Yoshida, Y. (1983b): Geological map of Sinnan Rocks, Antarctica. Antarct. Geol. Map Ser., Sheet 14 (with explanatory text 7 p.). Tokyo, Natl Inst. Polar Res.

Hiroi, Y., Shiraishi, K., Motoyoshi, Y., Kanisawa, S., Yanai, K. and Kizaki, K. (1986): Mode of occurrence, bulk chemical compositions, and mineral textures of ultramafic rocks in the Lützow-Holm Complex, East Antarctica. Mem. Natl Inst. Polar Res., Spec. Issue, **43**, 62–84.

Hiroi, Y., Shiraishi, K., Motoyoshi, Y. and Katsushima, T. (1987): Progressive metamorphism of calc-silicate

rocks from the Prince Olav and Sôya Coasts, East Antarctica. Proc. NIPR Symp. Antarct. Geosci., **1**, 73–97.

Hiroi, Y., Shiraishi, K. and Motoyoshi, Y. (1991): Late Proterozoic paired metamorphic complexes in East Antarctica, with special reference to the tectonic significance of ultramafic rocks. Geological Evolution of Antarctica, ed. by M.R.A. Thomson *et al.* Cambridge, Cambridge Univ. Press, 83–87.

Hiroi, Y., Motoyoshi, Y., Satish-Kumar, M., Kagashima, S., Suda, Y. and Ishikawa, N. (2006): Granulites from Cape Hinode in the amphibolite-facies eastern part of Prince Olav Coast, East Antarctica: New evidence for allochthonous block in the Lützow-Holm Complex. Polar Geosci., **19**, 89–108.

Ichiyama, Y. and Ishiwatari, A. (2004): Petrochemical evidence for off-ridge magmatism in a back-arc setting from the Yakuno ophiolite, Japan. Isl. Arc, **13**, 157–177.

Ishiwatari, A., Ikeda, Y. and Koide, Y. (1991): The Yakuno ophiolite, Japan: fragment of Permian island arc and marginal basin crust with a hotspot. Ophiolites, Oceanic Crustal Analogues, ed. by J. Malpas *et al.* Cyprus, Geological Survey Department, 497–506.

Ishizuka, H. (1981): Geochemistry of the Horokanai ophiolite in the Kamuikotan tectonic belt, Hokkaido, Japan. J. Geol. Soc. Jpn., **87**, 17–34 (in Japanese with English abstract).

Jacobs, J. and Thomas, R.J. (2004): Himalayan-type indenter-escape tectonic model for the southern part of the late Neoproterozoic–early Paleozoic East African–Antarctic orogen. Geology, **32**, 721–724.

Jacobs, J., Fanning, C.M., Henjes-Kunst, F., Olesch, M. and Paech, H.-J (1998): Continuation of the Mozambique Belt into East Antarctica: Grenville-age metamorphism and polyphase Pan-African high-grade events in Central Dronning Maud Land. J. Geol., **106**, 385–406.

Kanisawa, S., Yoshida, T. and Ishikawa, K. (1987): Preliminary study on trace element geochemistry of metabasites around Syowa Station and the adjacent areas. Proc. NIPR Symp. Antarct. Geosci., **1**, 98–106.

Kehelpannala, K.V.W. (2004): Arc accretion around Sri Lanka during the assembly of Gondwana. Gondwana Res., Suppl. Issue, **7**, 1323–1328.

Kerr, A.C., White, R.V. and Sunders, A.D. (2000): LIP Reading: recognizing oceanic plateaux in the geologic record. J. Petrol., **41**, 1041–1056.

Khan, M.S., Smith, T.E., Raza, M. and Huang, J. (2005): Geology, geochemistry and tectonic significance of mafic-ultramafic rocks of Mesopoterozoic Phulad ophiolite suite of South Delhi Fold Belt, NW Indian Shield. Gondwana Res., **8**, 553–566.

Kizaki, K., Hiroi, Y. and Kanisawa, S. (1983): Geological map of Niban Rock, Antarctica. Antarct. Geol. Map Ser., Sheet 17 (with explanatory text 5 p.). Tokyo, Natl Inst. Polar Res.

Koizumi, K. and Ishiwatari, A. (2006): Oceanic plateau accretion inferred from Late Paleozoic greenstones in the Jurassic Tamba accretionary complex, southwest Japan. Isl. Arc, **15**, 58–83.

Kriegsman, L.M. (1995): The Pan-African event in East Antarctica: a view from Sri Lanka and the Mozambique Belt. Precambrian Res., **109**, 25–38.

Leake, B.E., Woolley, A.R., Arps, C.E.S., Birch, W.D., Gilbert, M.C., Grice, J.D., Hawthorne, F.C., Kato, A., Kisch, H.J., Krivovichev, V.G., Linthout, K., Lard, J. and Mandarino, J. (1997): Nomenclature of amphiboles: report of the subcommittee of the international mineralogical association, commission on new minerals and mineral names. Mineral. Mag., **61**, 295–321.

Le Bas, M.J. (2000): IUGS reclassification of the high-Mg and picritic volcanic rocks. J. Petrol., **41**, 1467–1470.

Meert, J. (2003): A synopsis of events related to the assembly of eastern Gondwana. Tectonophysics, **362**, 1–40.

Meschede, M. (1986): A method of discriminating between different types of mid-ocean-ridge basalts and continental tholeiites with the Nb-Zr-Y diagram. Chem. Geol., **56**, 207–218.

Miyashiro, A. (1975): Classification, characteristics, and origin of ophiolites. J. Geol., **83**, 249–281.

Motoyoshi, Y. (1986): Prograde and progressive metamorphism of the granulite-facies Lützow-Holm Bay region, East Antarctica. D.Sc. Thesis, Hokkaido University, 238 p.

Motoyoshi, Y. and Ishikawa, M. (1997): Metamorphic and structural evolution of granulites from Rundvågshetta, Lützow-Holm Bay, East Antarctica. The Antarctic Region: Geological Evolution and Processes, ed. by C.A. Ricci. Siena. Terra Antarct. Publ., 65–72.

Motoyoshi, Y. and Shiraishi, K. (1994): Quantitative chemical analyses of rocks with X-ray fluorescence

analyzer (1) Major elements. Nankyoku Shiryô (Antarct. Rec.), **39**, 40–48 (in Japanese with English abstract).

Motoyoshi, Y., Matsubara, H., Matsumoto, Y., Moriwaki, K., Yanai, K. and Yoshida, Y. (1985): Geological map of Strandnibba, Antarctica. Antarct. Geol. Map Ser., Sheet 26 (with explanatory text 10 p.). Tokyo, Natl Inst. Polar Res.

Motoyoshi, Y., Matsueda, H., Matsubara, S., Sasaki, K. and Moriwaki, K. (1986): Geological map of Rundvågskollane and Rundvågshetta, Antarctica. Antarct. Geol. Map Ser., Sheet 24 (with explanatory text 11 p.). Tokyo, Natl Inst. Polar Res.

Motoyoshi, Y., Ishizuka, H. and Shiraishi, K. (1996): Quantitative chemical analyses of rocks with X-ray fluorescence analyzer (2) Trace elements. Nankyoku Shiryô (Antarct. Rec.), **40**, 53–63 (in Japanese with English abstract).

Nagahashi, T. and Miyashita, S. (2002): Petrology of the greenstones of the Lower Sorachi Group in the Sorachi–Yezo Belt, central Hokkaido, Japan, with special reference to discrimination between oceanic plateau basalts and mid-oceanic ridge basalts. Isl. Arc, **11**, 122–141.

Nakai, Y., Kano, T. and Yoshikura, S. (1980): Geological map of Cape Ryûgû, Antarctica. Antarct. Geol. Map Ser., Sheet 14 (with explanatory text 9 p.). Tokyo, Natl Inst. Polar Res.

Nakai, Y., Kano, T. and Yoshikura, S. (1981): Geological map of Oku-iwa Rock, Antarctica. Antarct. Geol. Map Ser., Sheet 22 (with explanatory text 4 p.). Tokyo, Natl Inst. Polar Res.

Nakajima, T., Shibata, K., Shiraishi, K., Motoyoshi, Y. and Hiroi, Y. (1987): Rb-Sr whole-rock age of the metamorphic rocks from eastern Queen Maud Land, East Antarctica. The 8th Symposium on Antarctic Geosciences, Program and Abstract. Tokyo, Natl Inst. Polar Res., 15 (in Japanese).

Nishi, N., Kawano, Y. and Kagami, H. (2002): Rb-Sr and Sm-Nd isotopic geochronology of the granitoid and hornblende biotite gneiss from Oku-iwa Rock in the Lützow-Holm Complex, East Antarctica. Polar Geosci., **15**, 46–65.

Nishida, T., Yanai, K., Kojima, H., Matsueda, H. and Kanisawa, S. (1984): Geological map of Kasumi Rock, Antarctica. Antarct. Geol. Map Ser., Sheet 18 (with explanatory text 6 p.). Tokyo, Natl Inst. Polar Res.

Osanai, Y., Shiraishi, K., Takahashi, Y., Ishizuka, H., Taninosho, Y., Tsuchiya, N., Sakiyama, T. and Kodama, S. (1992): Geochemical characteristics of metamorphic rocks from the central Sør Rondane Mountains, East Antarctica. Recent Progress in Antarctic Earth Science, ed. by Y. Yoshida *et al.* Tokyo, Terra Sci. Publ., 17–27.

Osanai, Y., Toyoshima, T., Owada, M., Tsunogae, T., Hokada, T., Crowe, W.A., Ikeda, T., Kawakami, T., Kawano, Y., Kawasaki, T., Ishikawa, M., Motoyoshi, Y. and Shiraishi, K. (2004): Geological map of Skallen, Antarctica (revised version). Antarct. Geol. Map Ser., Sheet 39 (with explanatory text 23 p.). Tokyo, Natl Inst. Polar Res.

Pearce, J.A. (1982): Trace element characteristics of lavas from destructive plate boundaries. Andesites, ed. by R.S. Thorpe. Wiley, Chichester, 525–548.

Pearce, J.A. and Gale, D.M. (1977): Identification of ore-deposition environment from trace-element geochemistry of associated igneous host rocks. Volcanic Processes in Ore Genesis, ed. by M.J. Jones. London, Geol. Soc., 14–29 (Geol. Soc. London, Spec. Publ., **7**).

Pearce, J.A. and Norry, M.J. (1979): Petrogenetic implication of Ti, Zr, Y, and Nb variations in volcanic rocks. Contrib. Mineral. Petrol., **69**, 33–47.

Rasse, P. (1974): Al and Ti contents of hornblende, indicators of pressure and temperature of regional metamorphism. Contrib. Mineral. Petrol., **45**, 231–236.

Rietmeijer, F.J.M. (1983): Chemical distinction between igneous and metamorphic orthopyroxenes especially those coexisting with Ca-rich clinopyroxenes: a re-evaluation. Mineral. Mag., **47**, 143–151.

Rollinson, H. (1993): Using Geochemical Data: Evaluation, Presentation, Interpretation. London, Longman, 352 p.

Shervais, J.W. (1982): Ti-V plots and the petrogenesis of modern and ophiolitic lavas. Earth Planet. Sci. Lett., **59**, 101–118.

Shiraishi, K. and Yoshida, M. (1987): Geological map of Botnneset, Antarctica. Antarct. Geol. Map Ser., Sheet 25 (with explanatory text 9 p.). Tokyo, Natl Inst. Polar Res.

Shiraishi, K., Hiroi, Y. and Onuki, H. (1984): Orthopyroxene-bearing rock from the Tenmondai and

Naga-iwa Rocks in the Prince Olav Coast, East Antarctica; first appearance of orthopyroxene in progressive metamorphic sequence. Mem. Natl Inst. Polar Res., Spec. Issue, **33**, 126–144.

Shiraishi, K., Hiroi, Y., Moriwaki, K., Sakai, K. and Onuki, H. (1985): Geological map of Tenmondai Rock, Antarctica. Antarct. Geol. Map Ser., Sheet 19 (with explanatory text 7 p.). Tokyo, Natl Inst. Polar Res.

Shiraishi, K., Ellis, D.J., Hiroi, Y., Fanning, Y., Motoyoshi, Y. and Nakai, Y. (1994): Cambrian Orogenic Belt in East Antarctica and Sri Lanka: implications for Gondwana Assembly. J. Geol., **102**, 47–65.

Shiraishi, K., Kagami, H. and Yanai, K. (1995): Sm-Nd and Rb-Sr isochron ages for meta-trondhjemites from Cape Hinode. Proc. NIPR Symp. Antarct. Geosci., **8**, 130–136.

Shiraishi, K., Hokada, T., Fanning, C.M., Misawa, K. and Motoyoshi, Y. (2003): Timing of thermal events in eastern Dronning Maud Land. Polar Geosci., **16**, 76–99.

Shuto, K. and Osanai, Y. (2002): Kisai-Gansekigaku, Ge. Tokyo, Kyoritsu Shuppan, 260 p. (in Japanese).

Stern, R.J. (1994): Arc assembly and continental collisions in the Neoproterozoic East African orogen: implications for the consolidation of Gondwana. Annu. Rev. Earth Planet. Sci., **22**, 319–351.

Storey, M., Kent, R.W., Saunders, A.D. *et al.* (1992): Lower Cretaceous volcanic rocks on continental margins and their relationship to the Kerguelen Plateau. Proc. Ocean Drill. Program, Sci. Results, **120**, 33–53.

Sun, S.S. and McDonough, W.F. (1989): Chemical and isotopic systematics of oceanic basalts: implications for mantle composition and processes. Magmatism in the Ocean Basin, ed. by A.D. Saunders and M. Norry. London, Geol. Soc., 313–345 (Geol. Soc. London, Spec. Publ., **42**).

Ueda, H., Kawamura, M. and Niida, K. (2000): Accretion and tectonic erosion processes revealed by the mode of occurrence and geochemistry of greenstones in the Cretaceous accretionary complexes of the Idonnappu Zone, southern central Hokkaido, Japan. Isl. Arc. **9**, 237–257.

Wilson, T.J., Grunow, A.M. and Hanson, R.E. (1997): Gondwana assembly: the view from Southern Africa and East Gondwana. J. Geodyn., **23**, 263–286.

Winchester, J.A. and Floyd, P.A. (1976): Magma type and tectonic setting discrimination using immobile elements. Earth Planet. Sci. Lett., **28**, 459–469.

Winkler, H.G.F. (1979): Petrogenesis of Metamorphic Rocks. New York, Springer, 334 p.

Yanai, K., Kizaki, K., Tatsumi, T. and Kikuchi, T. (1974a): Geological map of East Ongul Island, Antarctica. Antarct. Geol. Map Ser., Sheet 1 (with explanatory text 13 p.). Tokyo, Natl Inst. Polar Res.

Yanai, K., Tatsumi, T. and Kikuchi, T. (1974b): Geological map of West Ongul Island, Antarctica. Antarct. Geol. Map Ser., Sheet 2 (with explanatory text 5 p.). Tokyo, Natl Inst. Polar Res.

Yanai, K., Kizaki, K., Shiraishi, K., Hiroi, Y. and Kanisawa, S. (1984): Geological map of Akarui Point and Naga-iwa Rock, Antarctica. Antarct. Geol. Map Ser., Sheet 20 (with explanatory text 6 p.). Tokyo, Natl Inst. Polar Res.

Yoshida, M. (1978): Tectonics and petrology of charnockites around Lützow-Holmbukta, East Antarctica. J. Geosci., Osaka City Univ., **21**, 65–152.

Yoshida, M., Yoshida, Y., Ando, H., Ishikawa, T. and Tatsumi, T. (1976): Geological map of Skallen, Antarctica. Antarct. Geol. Map Ser., Sheet 9 (with explanatory text 16 p.). Tokyo, Natl Inst. Polar Res.

Yoshimura, Y., Motoyoshi, Y., Miyamoto, T., Grew, E.S., Carson, C.J. and Dunkley, D.J. (2004): High-grade metamorphic rocks from Skallevikhalsen in the Lützow-Holm Complex, East Antarctica: metamorphic conditions and possibility of partial melting. Polar Geosci., **17**, 57–87.